Tau in cerebrospinal fluid induces neuronal hyperexcitability and alters hippocampal theta oscillations

Jessica Brown[1,2], Elena Camporesi[3], Juan Lantero-Rodriguez[3], Maria Olsson[3,4], Alice Wang[1], Blanca Medem[1], Henrik Zetterberg[3,4,6,7,8,9], Kaj Blennow[3,4], Thomas K. Karikari[3,4,5], Mark Wall[1] and Emily Hill[1*]

1. *School of Life Sciences, University of Warwick, Coventry, CV4 7AL, UK*
2. *Division of Pharmacy and Optometry, School of Health Sciences, Faculty of Biology, Medicine and Health, University of Manchester, M13 9PL*
3. *Department of Psychiatry and Neurochemistry, Institute of Neuroscience and Physiology, University of Gothenburg, SE-43180, Mölndal, Sweden*
4. *Clinical Neurochemistry Laboratory, Sahlgrenska University Hospital, SE-43180, Mölndal, Sweden*
5. *Department of Psychiatry, School of Medicine, University of Pittsburgh, Pittsburgh 15213, PA, USA*
6. *UK Dementia Research Institute at UCL, London, WC1E 6BT, UK*
7. *Department of Neurodegenerative Disease, UCL Institute of Neurology, London, WC1E 6BT, UK*
8. *Hong Kong Center for Neurodegenerative Diseases, Clear Water Bay, Hong Kong, China*
9. *Wisconsin Alzheimer's Disease Research Center, University of Wisconsin School of Medicine and Public Health, University of Wisconsin-Madison, Madison, WI 53792, USA*

** Corresponding author: Dr Emily Hill, E.hill.4@warwick.ac.uk*

Key Words: Tau, Electrophysiology, Cerebrospinal fluid, Tauopathy, Theta oscillations

Abstract

Alzheimer's disease (AD) and other tauopathies are characterized by the aggregation of tau into soluble and insoluble forms (including tangles and neuropil threads). In humans, a fraction of both phosphorylated and non-phosphorylated N-terminal to mid-domain tau species, including the aggregated forms, are secreted into cerebrospinal fluid (CSF). Some of these CSF tau species can be measured as diagnostic and prognostic biomarkers, starting from early stages of disease. While in animal models of AD pathology, soluble tau aggregates have been shown to disrupt neuronal function, it is unclear whether the tau species present in CSF will modulate neural activity. Here, we have developed and applied a novel approach to examine the electrophysiological effects of CSF from patients with a tau-positive biomarker profile. The method involves incubation of acutely-isolated wild-type mouse hippocampal brain slices with small volumes of diluted human CSF, followed by a suite of electrophysiological recording methods to evaluate their effects on neuronal function from single cells through to the network level. Comparison of the toxicity profiles of the same CSF samples, with and without immuno-depletion for tau, has enabled a pioneering demonstration that CSF-tau potently modulates neuronal function. We demonstrate that CSF-tau mediates an increase in neuronal excitability in single cells. We then observed, at the network level, increased input-output responses and enhanced paired-pulse facilitation as well as an increase in long-term potentiation. Finally, we show that CSF-tau modifies the generation and maintenance of hippocampal theta oscillations, which have important roles in learning and memory and are known to be altered in AD patients. Together, we describe a novel method for screening human CSF-tau to understand functional effects on neuron and network activity, which could have far-reaching benefits in understanding tau pathology, thus allowing for the development of better targeted treatments for tauopathies in the future.

Graphic Abstract

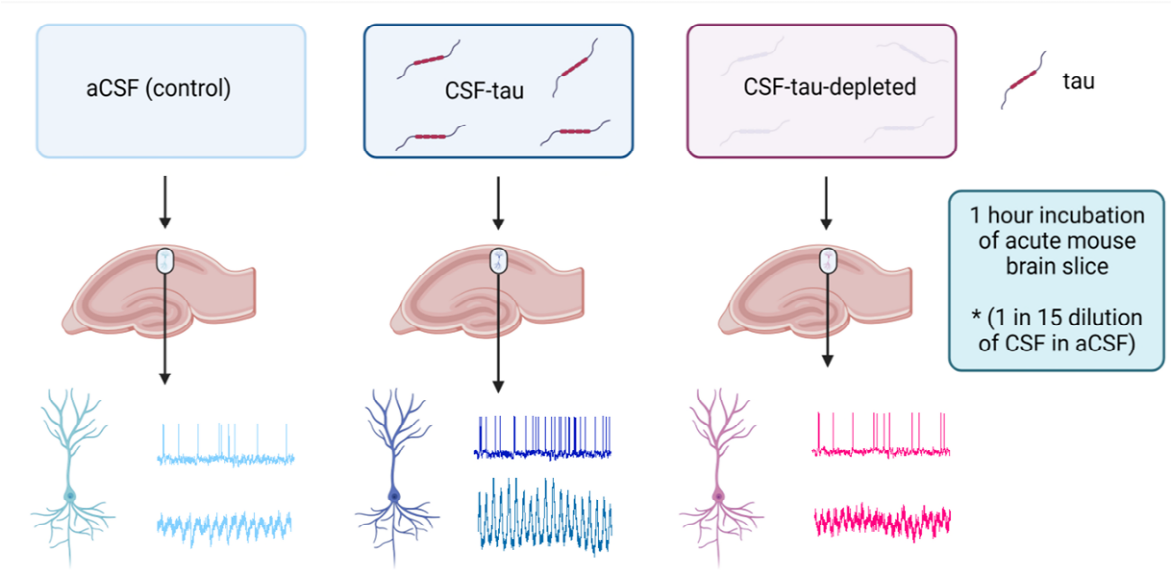

1. Introduction

Tau plays a central role in the neuropathology of Alzheimer's disease (AD) and other tauopathies [67, 110]. Whilst insoluble high-molecular weight tau aggregates, including neurofibrillary tangles are more prominent in late phases of these diseases and can help stage their pathological and clinical severity [20, 29, 92], the soluble forms of tau, including low-molecular weight aggregated and phosphorylated forms, are thought to be the most toxic species that modulate changes in neuronal function in the early stages of disease. In animal models of AD pathology, soluble tau aggregates have been shown to disrupt neuronal function, alter synaptic plasticity and impair cognitive function [19, 43, 79, 102, 105].

In AD,N-terminal to mid-domain tau fragments, both phosphorylated and non-phosphorylated variants, are released into the cerebrospinal fluid (CSF) early in disease progression, which has enabled the development of biomarkers for disease prognosis, diagnosis, and staging [18, 31, 55, 65, 107, 108]. While the presence of different tau forms in the CSF of AD patients is associated with neurofibrillary tangle pathology and cognitive decline [17, 28, 48, 62, 72, 87, 113], it is currently unclear whether the tau present in CSF is functionally active and can therefore modulate neural activity.

We have previously developed a technique using whole-cell patch-clamp recording to introduce structurally-defined soluble full-length recombinant tau aggregates into single neurons [58–60]. Using this approach, we have been able to provide detailed characterisation of the pathological actions of soluble tau aggregates on single neuron electrophysiology, evaluate changes to synaptic transmission and plasticity, and demonstrate that the effects are specific to the aggregates as monomers had little or no effect [58, 59]. However, a limitation of using recombinantly produced tau is that it cannot represent the full range of endogenous tau forms present in the disease and delivery via a patch-pipette will only target a single neuron, thus, it is not possible to determine how these changes will modulate brain network function. To overcome these drawbacks, we have developed a new approach of

incubating cortical slices in dilutions of patient CSF, which has allowed us to examine effects of clinically derived tau species on single neurons and on cortical network activity (theta oscillations).

Active cortical networks support several rhythms (such as gamma and theta oscillations) that can be measured clinically including in individuals suspected to be affected by AD. Theta oscillations (4 – 7 Hz) represent the largest extracellular signal recorded in the mammalian brain [124] and are considered integral to hippocampal learning and memory processes [13, 15, 51]. Specifically, activity within the theta band reflects the temporal encoding of information and is thus associated with the consolidation and retrieval of episodic and spatial memory [82, 127]. Work on both rodent models of AD and human AD patients has shown that these rhythms and their coupling are disrupted as the pathology progresses [45, 64, 89, 90, 98, 109, 111]. In humans, changes in theta power have been widely reported during the performance of spatial navigation, working memory and recognition tasks [21, 25, 34, 40, 75, 103].

In this study, we have characterised the functional neurotoxic changes induced by tau-positive CSF samples, on neuronal function. We have used a suite of detailed electrophysiological measures; from single cells to network activity. We demonstrate that CSF-tau mediates an increase in neuronal excitability, alters synaptic transmission and plasticity and modifies the generation and maintenance of hippocampal theta oscillations. However, the same CSF samples, with tau removed by immuno-depletion, failed to produce these effects, indicating that tau is central to these neural changes.

2. Materials and methods

2.1 Collection, biomarker profiling and immuno-depletion of CSF

All CSF samples were obtained from patients by lumbar puncture from the L3/L4 or the L4/L5 inter-space in the morning, according to standardized procedure. Samples were collected in a propylene tube and centrifuged for 10 min at 1800 x g at + 4 °C. The supernatant was stored at – 80 °C prior to use. The CSF samples used in this study were the remainder following clinical routine analyses, from multiple de-identified patients, pooled together in a procedure approved by the Ethics Committee at the University of Gothenburg (#EPN 140811). The collection and use of CSF samples were in accordance with the Swedish law of biobank in healthcare (2002:297).

The biomarker profile for the pool, including Aβ42, Aβ40, total tau (t-tau) and phosphorylated tau at threonine 181 (p-tau181), was measured with the fully automated Lumipulse (Fujirebio) platform following published protocols [49]. The CSF pool was then divided into two equal aliquots. To remove tau protein, aliquot 1 was immuno-depleted using immunoprecipitation (IP) following a previously established protocol [77] combining three antibodies to thoroughly cover across the full-length tau-441 sequence. Four µg of Tau12 (N-terminal [epitope = amino acids 6-18], BioLegend), HT7 (mid-region [epitope = amino acids 159-163], ThermoFisher), and TauAB (C-terminal [epitope = amino acids 425-441], kindly provided by MedImmune) were independently conjugated with 50 µL of M-280 Dynabeads (sheep anti-mouse IgG, Invitrogen) following manufacturer's recommendations. Beads were then mixed and added to aliquot 1. Incubation was performed overnight at 4 °C on a rolling station to allow mixing of the beads with the sample and to avoid the beads forming aggregated deposits. The next morning,

the beads were removed from the mixture by standing the tube against a magnet. The supernatant was carefully pipetted out to obtain the CSF-tau-depleted fraction. Aliquot 2 underwent the same free-thaw cycle as the CSF-tau-depleted but was not immuno-depleted. Both samples were stored at –80 °C prior to use. To verify the removal of tau after the immuno-depletion, we used different assays that cover various regions of tau. The t-tau assay from Quanterix, p-tau181 [73] and p-tau231 [8] in house assays were used for tau measurements in both the CSF-depleted and the non-depleted aliquots on a Simoa HD-X instrument (Quanterix, Billerica, MA, USA) following methods originally described in the cited publications. To further validate the removal of tau, the CSF-depleted sample was also tested using the mid-region targeting Lumipulse p-tau-181 assay (Fujirebio) [49].

CSF collection and processing were performed at the University of Gothenburg, Sweden, with local ethical approval, and the samples sent to the University of Warwick, UK, where all experiments were done as approved by the local Human Tissue Authority and Biomedical & Scientific Research Ethics Committees.

2.4 Preparation of mouse brain slices

All animal care and experimental procedures were reviewed and approved by the institutional animal welfare and ethical review body (AWERB) at the University of Warwick. Animals were kept in standard housing with littermates, provided with food and water ad libitum and maintained on a 12:12 (light-dark) cycle. C57BL/6 mice (3–4-week-old; male and female) were killed by cervical dislocation and decapitated in accordance with the United Kingdom Animals (Scientific Procedures) Act (1986). The brain was rapidly removed, and acute parasagittal or horizontal brain slices (350-400 µm) were cut with a Microm HM 650V microslicer in cold (2–4°C) high Mg^{2+}, low Ca^{2+} artificial CSF (aCSF), composed of the following: 127 mM NaCl, 1.9 mM KCl, 8 mM $MgCl_2$, 0.5 mM $CaCl_2$, 1.2 mM KH_2PO_4, 26 mM $NaHCO_3$, and 10 mM D-glucose (pH 7.4 when bubbled with 95% O_2 and 5% CO_2, 300 mOsm). Slices were stored at 34°C in standard aCSF (1 mM Mg^{2+} and 2 mM Ca^{2+}) for between 1 and 8 hours.

2.5 Incubation of acute brain slices with CSF samples

After at least 1 hour of recovery, slices were either incubated in aCSF (control) or in varying dilutions (1:15, 1:30, 1:100 in aCSF) of CSF-tau or CSF-tau-depleted (immunodepleted for tau) for 1 hour, in bespoke incubation chambers at room temperature. The incubation chambers consisted of small, raised grids (to allow perfusion of slices from above and below) placed in the wells of a twenty-four well plate (Falcon) which were bubbled with 95 % O_2, 5 % CO_2 using microloaders (Eppendorf). Slices were placed into the incubation chambers one at a time (minimum volume 1.5 ml to cover raised grid). Individual slices were then placed on the recording rig and perfused with regular aCSF throughout the recording period, so the CSF-tau was only present for the 1-hour incubation.

2.6 Whole cell patch clamp recording from single hippocampal CA1 pyramidal neurons

A slice was transferred to the recording chamber, submerged, and perfused (2–3 ml/min) with aCSF at 30°C. Slices were visualised using IR-DIC optics with an Olympus BX151W microscope (Scientifica) and a CCD camera (Hitachi). Whole-cell current-clamp recordings were made from pyramidal cells in area CA1 of the hippocampus using patch pipettes (5–10 MΩ) manufactured from thick-walled glass (Harvard Apparatus). Pyramidal cells were identified by their position in the slice, morphology (from fluorescence imaging) and characteristics of the standard step current−voltage relationship. Voltage recordings were made using an Axon Multiclamp 700B amplifier (Molecular Devices) and digitised at 20 kHz. Data acquisition and analysis were performed using pClamp 10 (Molecular Devices). Recordings from neurons that had a resting membrane potential of between –55 and –75 mV at whole-cell breakthrough were accepted for analysis. The bridge balance was monitored throughout the experiments and any recordings where it changed by >20% were discarded.

Stimulation protocols

To extract the electrophysiological properties of recorded neurons, both step, ramp and more naturalistic, fluctuating currents were injected.

Standard IV protocol

The standard current−voltage relationship was constructed by injecting standard (step) currents from –200 pA incrementing by either 50 or 100 pA (1 s duration) until a regular firing pattern was induced. A plot of step current against voltage response around the resting potential was used to measure the input resistance (from the gradient of the fitted line).

Rheobase ramp protocol

To evaluate the rheobase (the minimum current required to elicit an action potential (AP)) a current ramp was injected into neurons. From the baseline, a 100 ms duration ramp to −100 pA was followed by a 900 ms duration ramp at 0.33 pA/ms up to 200 pA, then a step back down to baseline (zero current).

Dynamic IV protocol

The dynamic-I-V curve, defined by the average transmembrane current as a function of voltage during naturalistic activity, can be used to efficiently parameterize neurons and generate reduced neural models that accurately mimic the cellular response. The method has been previously described [10, 11, 56], for the dynamic-IV computational code, see [56]. Briefly, a current wave form, designed to provoke naturalistic fluctuating voltages, was constructed using the summed numerical output of two Ornstein–Uhlenbeck processes [121] with time constants τfast = 3 ms and τslow = 10 ms. This current waveform, which mimics the stochastic actions of AMPA and GABA-receptor channel activation, is injected into cells and the resulting voltage recorded (a fluctuating, naturalistic trace). The voltage trace was used to measure the frequency of action potential firing and to construct a dynamic-I-V curve. The firing rate was measured from voltage traces evoked by injecting a current wave form of the same gain for all recordings (to give a firing rate of ~2–3 Hz). Action potentials were detected by a manually set threshold

and the interval between action potentials measured. Dynamic I-V curves were constructed and used to extract a number of parameters including the capacitance, time constant, input resistance, resting membrane potential, spike threshold and spike onset (Fig. 2; [10, 11]). Using these parameters in a refractory exponential integrate-and-fire (rEIF) model reliably mimics the experimental data, with a spike prediction of ~70–80% as shown previously [10, 11]. All analyses of the dynamic-I-V traces were completed using either MATLAB or Julia software platforms [16].

2.7 Recording and analysing miniature excitatory postsynaptic currents (mEPSCs)

AMPA receptor-mediated miniature excitatory postsynaptic currents (mEPSCs) were recorded as previously described [37]. To isolate AMPA-mediated mEPSCs, aCSF contained 1 µM TTX, 50 µM picrotoxin to block $GABA_A$ receptors and 5 µM L689,560 to block NMDA receptors. Recordings of mEPSCs were obtained at a holding potential of −60 mV using an Axon Multiclamp 700B amplifier (Molecular Devices), filtered at 3 kHz and digitised at 20 kHz (Digidata 1440A, Molecular Devices). Data acquisition was performed using pClamp 10 (Molecular Devices). Analysis of mEPSCs was performed using MiniAnalysis software (SynaptoSoft). Events were manually analysed and were accepted if they had amplitude >6 pA (events below this amplitude were difficult to distinguish from baseline noise) and had a faster rise than decay. Statistical significance was measured using a one-way ANOVA.

2.8 Extracellular recording of synaptic transmission and plasticity

A 400 µM parasagittal slice was transferred to the submerged recording chamber and perfused with aCSF at 4-6 ml/min (32°C). The slice was placed on a grid allowing perfusion above and below the tissue and all tubing (Tygon) was gas tight (to prevent loss of oxygen). To record field excitatory postsynaptic potentials (fEPSPs), an aCSF-filled microelectrode was placed on the surface of stratum radiatum in CA1. A bipolar concentric stimulating electrode (FHC) controlled by an isolated pulse stimulator model 2100 (AM Systems, WA) was used to evoke fEPSPs at the Schaffer collateral–commissural pathway. Field EPSPs were evoked every 30 s (0.03 Hz). Stimulus input/output curves for fEPSPs were generated using stimulus strength of 1-5 V for all slices (stimulus duration 200 µs). For the synaptic plasticity experiments, the stimulus strength was set to produce a fEPSP slope ~ 40 % of the maximum response and a 20-minute baseline was recorded before plasticity induction. Paired-pulse facilitation was measured over an interval range of 20 to 500 ms. Long-term potentiation (LTP) was induced by high frequency stimulation (HFS, 100 stimuli in 1s, 100 Hz) and then fEPSPs were recorded for 60 minutes following LTP induction. Signals were filtered at 3 kHz and digitised on-line (10 kHz) with a Micro CED (Mark 2) interface controlled by Spike software (Vs 6.1, Cambridge Electronic Design, Cambridge UK). The fEPSP slope was measured from a 1 ms linear region following the fibre volley.

2.9 Theta Oscillations

2.9.1 Induction of theta oscillations in CA3

A 400 µM horizontal slice was transferred to an interface recording chamber (Digitimer BSC3) and placed on a mesh support at the interface of an oxygen-rich atmosphere and underlying aCSF. The temperature of the aCSF was set at 31°C and the flow rate was 1.5 ml/min. An aCSF-filled glass microelectrode was placed in CA3 to record activity. Baseline activity was recorded for 20 minutes before the bath application of the acetylcholine receptor agonist carbachol, selected to induce oscillations given the evidenced role of acetylcholine receptors in regulating hippocampal-dependent oscillations [7, 119]. Carbachol was applied at 50 µM, a concentration previously demonstrated to induce CA3 theta activity in rodent slices [3, 44, 70, 126]. Theta oscillations were recorded for 30 minutes with a differential amplifier (Warner instrument DP-301) with filter settings: low pass 3KHz, high pass 1Hz, amplification x1000). Data was acquired at a sampling rate of 10 KHz with a Micro1401 (Cambridge Electronic Design) using Spike 2 software.

2.9.2 Analysis of theta oscillations

Carbachol-elicited oscillations were characterised using power spectral density (PSD) analysis in Spike 2. PSD profiles of the field potential recordings filtered for the theta band (4 – 7 Hz) were generated by Fourier transform analysis (Hanning window, FFT size 2048, resolution 4.883 Hz). The profiles were calculated from a 100 – 300 second section of the field potential trace displaying peak oscillatory activity, with the baseline power subtracted offline (supplementary figure 2). Recordings from slices from each treatment condition (control, CSF-tau and CSF-tau-depleted) were conducted in a random order each day to prevent any time effects, and a slice was only included in the analysis if robust oscillations were evoked. Differences between the three treatment groups (control, n = 8; CSF-tau, n = 8; CSF-tau-depleted, n = 8) in mean oscillatory power (mV^2) were compared using a Kruskal-Wallis test followed by a Dunn's multiple comparisons test. The peak oscillatory power of each trace (n=8 per group) was also compared with the corresponding baseline (n = 8 per group) within each treatment group and mean differences assessed using Wilcoxon tests. Finally, the mean time period (latency, seconds) from application of carbachol to the onset of oscillatory activity was compared between treatment groups using a Kruskal-Wallis test followed by a Dunn's multiple comparisons test.

2.10 Drugs

Picrotoxin (PTX; Sigma), carbachol (carbamoylcholine chloride; Sigma), Tetrodotoxin (TTX; Sigma) and trans-2-carboxy-5,7-dichloro-4-phenylaminocarbonylamino-1,2,3,4-tetrahydroquinoline (L689,560; Hello-Bio) were made up as stock solutions (1-50 mM) in distilled water or dimethyl sulfoxide (DMSO) and then diluted in aCSF on the day of use. The concentration of DMSO did not exceed 0.1 % in the final solutions.

2.11 Statistical Analysis

Statistical analysis was performed using GraphPad Prism. Due to small sample sizes ($n < 15$), statistical analysis was performed using non-parametric methods; Kruskal–Wallis analysis of variance (ANOVA), Mann–Whitney and Wilcoxon signed-rank tests as required. All data are represented as mean and standard error of the mean with individual experiments represented by single data points. For all experiments, significance was set at $p \leq 0.05$. Data points for each experimental condition were derived from a minimum of four individual animals.

3. Results

3.1 Characterisation of CSF-tau before and after the immuno-depletion for tau

To investigate the effects of CSF-tau on neuronal properties, in this proof-of-principle study, we used pooled CSF from multiple de-identified patients. The biomarker profile for the pool was measured with the Lumipulse platform. For the pooled samples used in this study, CSF Aβ1-42 level (469 pg/ml) was abnormal as it was below the clinically validated abnormality threshold of 526 pg/ml [48]. Aβ1-42/Aβ1-40 ratio was also in the positivity range (<0.072 pg/ml). T-tau (measured = 542 pg/ml) was above the abnormality threshold of 409 pg/ml [80] but p-tau181 remained negative [48]. These profiles suggest that pooled CSF sample was amyloid-positive, phosphorylated-tau-negative but neurodegeneration-positive (A+T-N+) [67].

To allow determination of the specific effects of tau on electrophysiological properties, an aliquot of the pooled CSF-tau sample was immuno-depleted for tau by the simultaneous application of the monoclonal antibodies Tau12, HT7 and TauAB (epitopes: amino acids 6-18, 159-163 and 425-441 respectively) that together cover a wide span of the tau-441 protein sequence. To confirm that tau removal protocols were effective, the immuno-depleted samples were reanalysed for t-tau, p-tau181 and ptau-231 using Simoa assays. P-tau181, p-tau231 and total-tau signals decreased by 86.9% and 92.4% and 83.8%, respectively. To further validate the depletion, p-tau181 was measured using a fully automated Lumipulse platform and the signal decreased by 80.5% (figure 1).

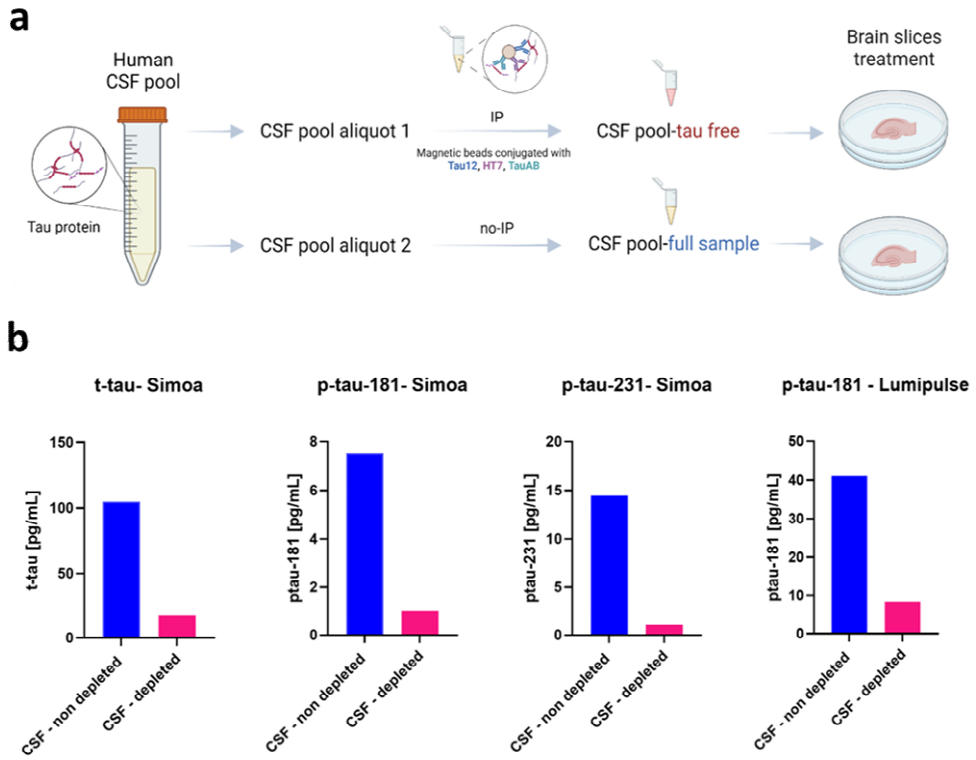

Figure 1. Immunodepletion of pooled CSF to remove tau using a combination of antibodies targeting the N terminus, mid region, and C terminus of tau. a. An aliquot of the pooled CSF-tau sample was immuno-depleted for tau by the simultaneous application of the monoclonal antibodies Tau12, HT7 and TauAB (epitopes: amino acids 6-18, 159-163 and 425-441, respectively) that together cover nearly the entire tau-441 protein sequence using published protocols [77] . **b**, To verify the removal of tau after the immuno-depletion, t-tau assay from Quanterix, p-tau181 [73] and p-tau231 [8] in house assays were used for tau measurements in both the CSF-depleted and non-depleted aliquots on a Simoa HD-X instrument (Quanterix, Billerica, MA, USA) following methods originally described in the cited publications and validated using fully automated Lumipulse (Fujirebio) platform following published protocols [49].

3.2 CSF-tau enhances hippocampal pyramidal neuronal excitability.

Tau aggregates have previously been reported both *in vitro* and *in vivo* to affect neuronal function, excitability, and synaptic plasticity [19, 43, 59, 79, 102, 105]. These tau-mediated deficits are largely mediated by soluble forms of the protein [59, 93, 112, 125], including those isolated from AD brains [78, 79]. However, studies using patient-derived CSF samples, which are estimated to contain a fraction of the soluble tau aggregates from AD brains [71, 87, 107], are lacking. Here, we investigated if the reported pathological effects of soluble tau aggregates can be reproduced with CSF-tau.

In this study, we used pooled CSF samples from multiple patients. The relatively large volume of pooled sample (5 ml) allowed us to perform a wide range of experiments using the same sample to fully characterise its neurotoxic effects. We diluted the CSF-tau sample with aCSF to reduce the volume of sample that was used for each experiment. As our eventual end goal will be to use individual patient samples (much smaller volumes ~300 µl) to enable correlation with clinical data, we first sought to find

the minimum volume (maximum dilution in aCSF) of CSF-tau, for which we could detect a change in neuronal function. We tested 1:100, 1:30 and 1:15 dilutions of the CSF-tau in aCSF. We used neuronal excitability, measured using whole-cell patch clamp recording from single CA1 pyramidal cells in the hippocampus, as the functional readout. We have previously found this to be a reliable and robust change induced by recombinant tau [58, 59]. We found no significant changes to neuronal excitability with either 1:100 dilution or 1:30 dilution of CSF-tau, but a significant depolarisation and increase in firing rate was observed with a 1:15 dilution (100 µl CSF in 1.5 ml aCSF; supplementary Figure 1). We therefore used a 1:15 dilution of CSF-tau and CSF-tau-depleted for all subsequent experiments. To fully evaluate the effects of CSF-tau at a single neuron level, slices were either incubated with CSF-tau (n = 11), CSF-tau-depleted (n = 10) or control aCSF (n = 10; no human sample) for 1 hour before recordings were made. Initially, standard current step protocols were used to measure passive neuronal parameters (see materials and methods for details).

Incubation with CSF-tau led to significant depolarisation of the resting membrane potential (RMP; mean RMP in control slices of -68 ± 0.92 mV compared to the mean RMP in CSF-tau of -63 ± 0.79 mV; *Figure 2a, b*), an effect that was not observed in slices incubated in CSF-tau-depleted (mean RMP of -69 ± 1.09 mV; *Figure 2a, b*). A Kruskal-Wallis test showed that the difference in RMP between the three treatment groups was significant (F*igure 2b*; H (2) = 14.98, $p < 0.0006$), with Dunn's tests revealing a significant depolarisation of the RMP following CSF-tau treatment relative to aCSF control slices ($p < 0.0121$) and treatment with CSF-tau-depleted ($p < 0.0008$), whilst there was no significant difference between control and CSF-tau-depleted groups ($p > 0.9999$).

Incubation with CSF-tau also significantly increased the input resistance (IR, reflecting a decrease in whole cell conductance). The mean IR in control slices was 143.6 ± 5.2 MΩ, compared to the mean IR in slices incubated in CSF-tau of 167 ± 7.2 MΩ; F*igure 2a, c*), an effect which again was not observed in slices incubated in CSF-tau-depleted (mean IR of 126 ± 9.9 mV; *Figure 2a, c*). The difference in IR between the three treatment groups was also significant (Kruskal Wallis test; *Figure 2c*; H (2) = 12.39, $p < 0.0020$), with Dunn's tests revealing a significant increase in IR following CSF-tau treatment relative treatment with CSF-tau-depleted ($p < 0.0013$), whilst there was no significant difference between either control (aCSF) and CSF-tau-depleted groups ($p < 0.2831$).

Given that CSF-tau depolarises the resting membrane potential and increases the IR, we predicted that it should also increase the action potential firing rate. To test this, we used a 40 s fluctuating naturalistic current injection (to mimic synaptic activation) and measured the firing rate. Incubation with CSF-tau significantly increased firing rate (FR). The mean FR in control was 2.3 ± 0.5 Hz compared to the mean FR in neurons exposed to CSF-tau of 4.2 ± 0.6 Hz; *Figure 2d, e*), This increase in FR was not observed in slices incubated in CSF-tau-depleted (mean FR of 2.1 ± 0.3 Hz; *Figure 2d, e*). A Kruskal-Wallis test showed that the difference in FR between the three treatment groups was also significant (*Figure 2e*; H (2) = 10.4, $p<0.0055$), with Dunn's tests revealing a significant increase in FR following CSF-tau treatment relative to aCSF control slices ($p < 0.0129$) and treatment with CSF-tau-depleted ($p < 0.0222$), whilst there was no significant difference between control and CSF-tau-depleted groups ($p > 0.9999$).

We have previously shown that tau aggregates decrease the rheobase (minimum current needed to fire an action potential; [58]), therefore we next checked whether the increase in excitability was accompanied by a change in rheobase (Figure 2f). The mean rheobase in neurons exposed to CSF-tau was significantly decreased (52 ± 6.6 pA) compared to aCSF control slices (87 ± 6.8 pA) or slices incubated in CSF-tau-depleted (74 ± 6.9 pA). A Kruskal-Wallis test showed that the difference in FR between the three treatment groups was also significant (*Figure 2g; H (2)* = 9.3, $p < 0.0093$), with Dunn's tests revealing a significant decrease in rheobase following CSF-tau treatment relative to aCSF control slices ($p = 0.0080$), whilst there was no significant difference between aCSF control and CSF-tau-depleted groups ($p = 0.8856$).

To determine if other neuronal parameters were significantly altered by CSF-tau, we used the dynamic IV method [10, 11] to measure capacitance, the time constant, the spike threshold and spike onset. Unlike our previous studies, using recombinant tau oligomers and associated truncations [58, 59], there were no significant differences in any of these parameters. We also evaluated whether there were changes to action potential amplitude or half-width, which we have previously observed with recombinant soluble tau aggregates [58, 59]. Again, we observed no significant changes to either of these parameters between the three conditions.

Thus, CSF-tau replicates a number of the pathological effects which have been reported previously in models of tauopathy. These effects were absent when tau was removed by immunodepletion, indicating that tau is critical to these disease-associated changes.

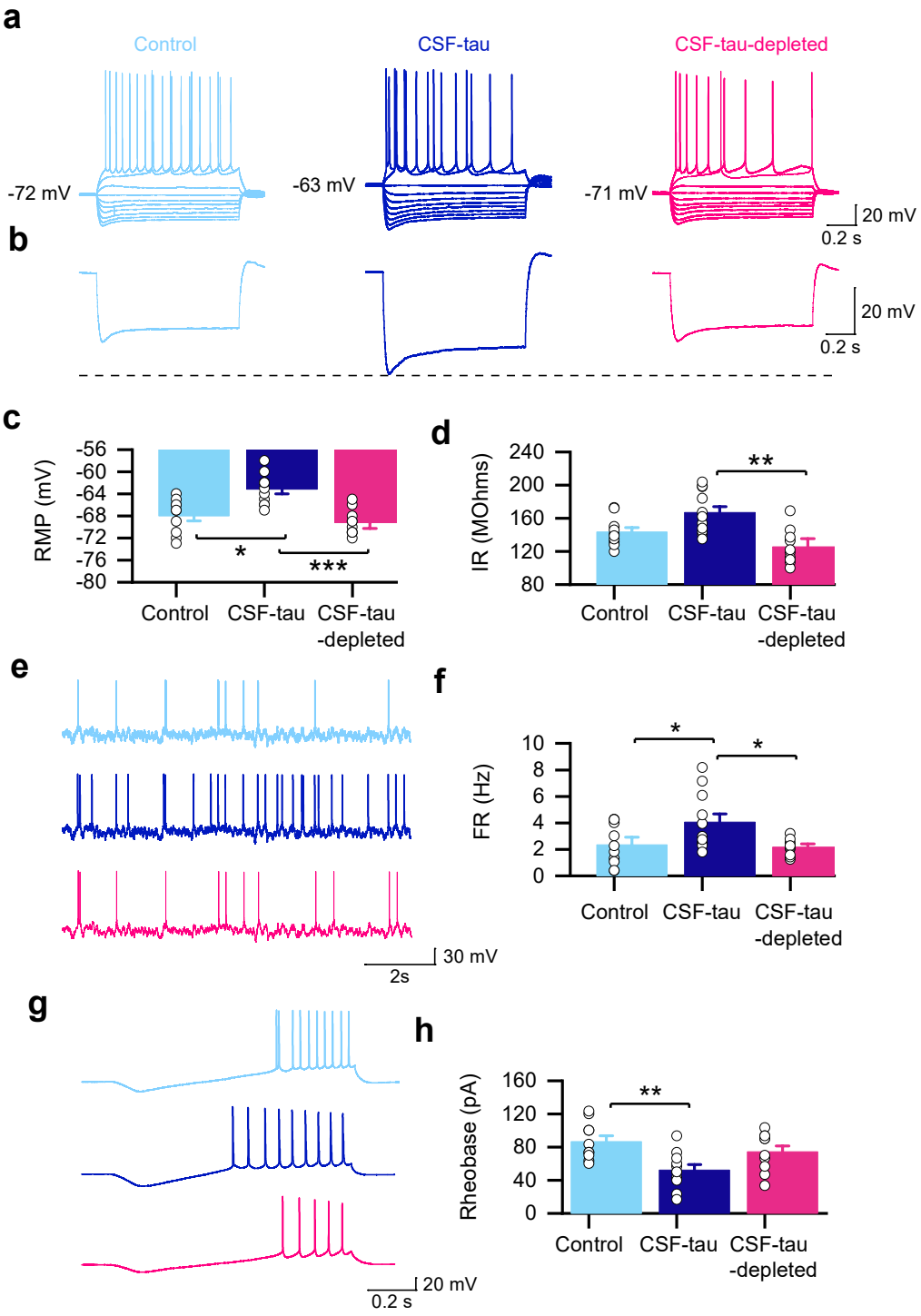

Figure 2. CSF-tau enhances hippocampal pyramidal neuronal excitability a. Representative examples of standard current-voltage responses for slices that have been incubated in control aCSF (light blue; n=10), CSF-tau (CSF; dark blue; n=11) or CSF-tau immunodepleted for tau (CSF-depleted; Pink; n=10). See Materials and Methods for incubation protocols. CSF-tau depolarised the resting membrane potential of the recorded neurons. **b**, the most negative step from traces in (**a**), clearly highlighting that CSF-tau also mediates an increase in input resistance. **c**, CSF-tau incubation resulted in a significant depolarisation of the resting membrane potential ($p < 0.0006$), which was not observed in the CSF sample immuno-depleted for tau. **d.** CSF-tau incubation also significantly increased input resistance ($p < 0.0020$), an effect which was also not observed in the CSF sample that

was immunodepleted for tau. **e.** Representative example of membrane-potential responses to naturalistic current injection for each of the three conditions. **f.** CSF-tau significantly increased the firing rate (a correlate of neuronal excitability; $p < 0.0055$). No change was observed with the CSF-tau sample immunodepleted for tau compared to control. **g.** The rheobase current (minimal current to evoke an AP) was determined by injecting a current ramp (−50 to 200 pA) and measuring the minimum current required to fire an action potential. **h.** CSF-tau incubation significantly decreased the rheobase ($p = 0.0093$). *Panels a, d and f show representative example traces and b, c, e, and g show the mean data and SEM, with individual datapoints overlaid.*

3.3 CSF-tau enhanced basal EPSP amplitude and paired pulse facilitation and long-term potentiation

Next, we investigated whether the changes to neuronal excitability in single pyramidal cells were accompanied by changes in synaptic transmission and plasticity in the CA1 region of the hippocampus.

Incubation in CSF-tau led to increased basal synaptic transmission, as measured by stimulus input/output curves (*Figure 3a*). For example, the mean fEPSP slope at 3 V in CSF-tau treated slices was 0.46 ± 0.06 mV/ms (n=8) compared to control slices which was 0.25 ± 0.04 mV/ms (n=10) and 0.22 ± 0.03 mV/ms in CSF-tau-depleted (n=12). A two-way ANOVA evaluating the fEPSP response to increasing stimulus across the three conditions showed a significant difference between the groups ($F(25, 225) = 15.05$, $p < 0.0001$) with significantly greater fEPSP slope for CSF-tau compared to CSF-tau-depleted at 2.5 mV ($p = 0.0486$), 3 mV ($p = 0.0241$) and 3.5 mV ($p = 0.0494$) stimulus strengths. We also measured the fibre volley for a given stimulus (4 mV) it found that it was significantly larger in CSF-tau (0.29 ± 0.03 mV) compared to control (0.15 ± 0.02 mV, $p=0.0278$)

We then examined whether there were changes to paired pulse facilitation (PPF). If the increase in fEPSP amplitude is a consequence of an increase in release probability, then it would be predicted that the degree of PPF would be reduced. However, the opposite was observed, and the degree of facilitation was significantly increased at 100 ms and 200 ms intervals (*Figure 3b*). For example, the mean paired-pulse ratio at a 100 ms interval in CSF-tau was 2.23 ± 0.1 compared to control aCSF which was 1.94 ± 0.07 and 1.87 ± 0.04 in CSF-tau-depleted. A two-way ANOVA evaluating the paired-pulse ratio at different intervals across the three conditions showed a significant difference between the groups ($F(2, 135) = 10.62$, $p< 0.0001$) with significantly greater facilitation for CSF-tau compared to CSF-tau-depleted at 100 ($p = 0.0081$) and 200 ms time intervals ($p = 0.0368$).

In the same recordings, we then examined whether CSF-tau altered long-term synaptic plasticity by recording long term potentiation (LTP) at the CA1 Schaffer collateral synapses. We measured the potentiation 60 minutes after HFS [61, 133] and found LTP to be significantly enhanced by CSF-tau. The mean potentiation (displayed as normalised fEPSP slope, *Figure 3c*) at 55-60 minutes after induction was 1.76 ± 0.09 in CSF-tau, in control aCSF it was 1.51 ± 0.06 and in CSF-tau-depleted it was 1.46 ± 0.07. A Kruskal Wallis test showed that the difference in potentiation between the three treatment groups was significant ($H (2) = 6.683$, $p = 0.0354$) with Dunn's tests revealing a significant increase in potentiation following CSF-tau treatment relative to treatment with CSF-tau-depleted ($p = 0.0415$), whilst there was no significant difference between control and CSF-tau-depleted groups ($p > 0.9999$).

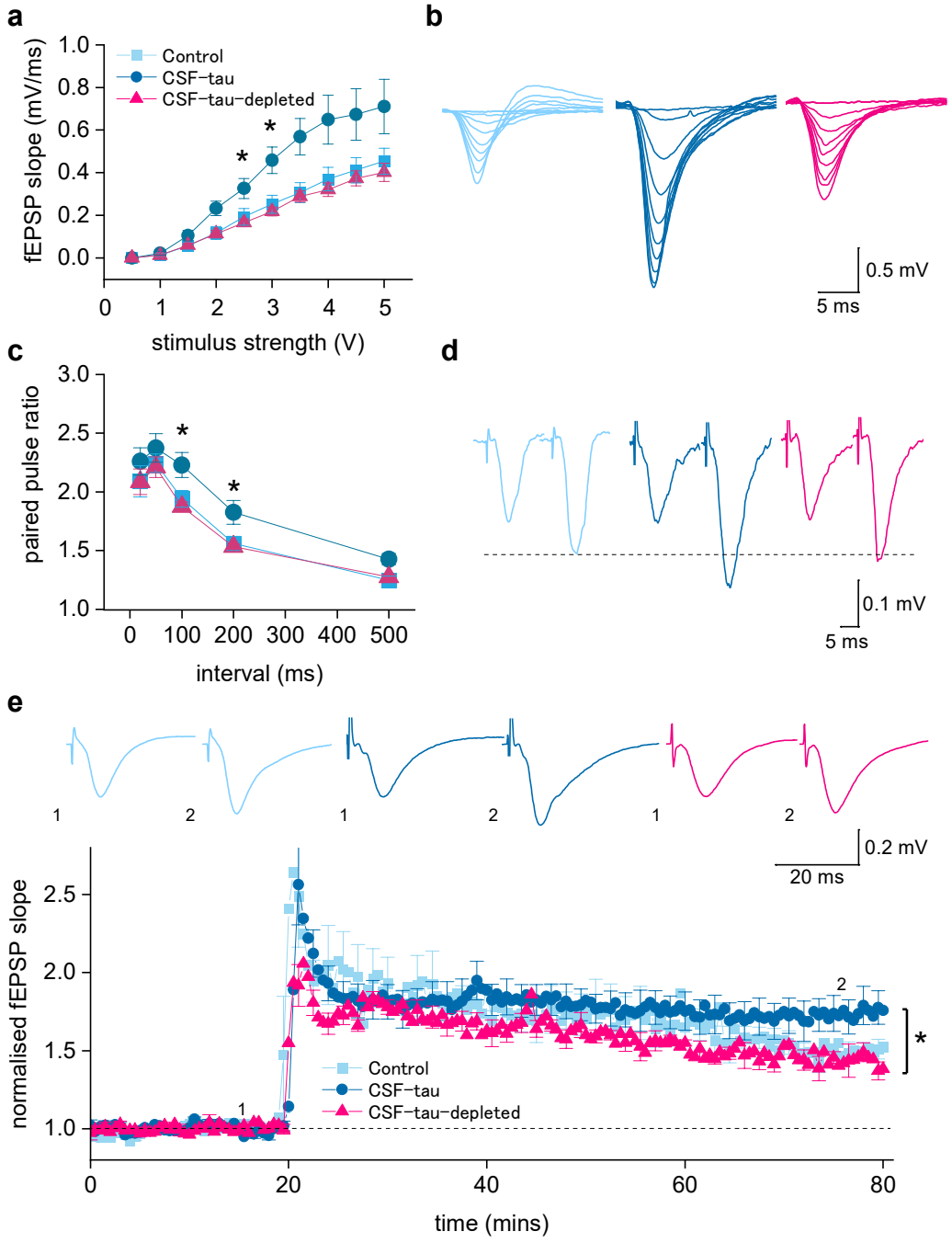

Figure 3. CSF-tau enhances basal synaptic transmission and synaptic plasticity. a. Graph plotting mean fEPSP slope against stimulus strength for control (n=10 slices), CSF-tau (n=11 slices) and CSF-tau-depleted (n=10 slices). **b**, Superimposed fEPSP waveforms at increasing stimulus strengths (0.5 to 5 V) for each of the three conditions. CSF-tau significantly enhanced fEPSP slope. **c,** Graph plotting mean paired pulse ratio against interval for all three conditions. CSF-tau significantly enhanced paired pulse facilitation. **d**, Representative example traces of fEPSP waveforms for the 200 ms interval for all three conditions. The first fEPSPs have been normalised so that facilitation can be compared across conditions **e,** Graph plotting mean normalised (to the baseline) fEPSP slope against time for all three conditions. After a 20-minute baseline, LTP was induced by HFS. Inset, example fEPSP waveforms before and after LTP induction (average of waveforms at 75-80 minutes). The mean potentiation was enhanced in CSF-tau. All Data is represented as Mean ± SEM.

3.4 Incubation with CSF-tau leads to an increase in the amplitude and frequency of mEPSCs

Since the increase in fEPSP amplitude did not appear to result from an increase in release probability, we hypothesised that it could result from an increase in synaptic AMPA receptor density. To evaluate whether there are changes in postsynaptic AMPA receptor currents, we used whole-cell voltage clamp recordings from CA1 pyramidal neurons to record AMPA receptor-mediated miniature EPSCs (mEPSCs) in the presence of PTX (to block $GABA_A$ receptors), L689,560 (to block NMDA receptors) and TTX (to block voltage gated Na channels).

We observed a significant increase in the frequency of mEPSCs (shorter interval between events) in the slices incubated with CSF-tau compared to control slices (*Figure 4a*). The distribution of intervals between events in CSF-tau was significantly different to that of control slices (Kolmogorov-Smirnov test; $D = 0.5494$, $p < 0.0001$, *Figure 4b*) with mEPSCs occurring at a much higher frequency in CSF-tau treated slices. On average the frequency was increased 7.5-fold compared to control recordings. Then, by comparing the mean mEPSC intervals between events for each slice across the two conditions, we further validated that slices incubated in CSF-tau showed significantly decreased intervals between events (increased frequency) compared to control slices (mean interval in CSF-tau was 1.9 ± 0.09 s vs mean interval in control was 17.6 ± 1.04 s; Mann-Whitney test p=0.0004; *Figure 4c*).

We also found that the amplitude of mEPSCs was significantly enhanced in CSF-tau incubated slices (*Figure 4d*). Using a Kolmogorov-Smirnov test to compare the cumulative frequency of the pooled mEPSCs for each of the conditions, we found that distribution of mEPSC amplitudes in slices exposed to CSF-tau (n=800 pooled mEPSCs from 8 slices) was significantly different to that of control slices (n=600 mEPSCs from 6 slices; $D = 0.1533$, $p < 0.0001$). Then, by comparing the mean mEPSC amplitudes for each slice across the two conditions, we further validated that slices incubated in CSF-tau showed increased amplitudes compared to control slices (mean amplitude in CSF was 22.5 ± 0.39 pA vs mean amplitude in control was 18.9 ± 0.33 pA; Mann-Whitney test $p = 0.0426$, *Figure 4e*).

Finally, to establish whether there were any changes to the kinetics of the mEPSCs, we then measured the rise and decay time for the average waveform from each recording. The rise time was measured (10-90%) and the decay time was obtained by fitting with a single exponential. There was no change to rise or decay kinetics between the two conditions.

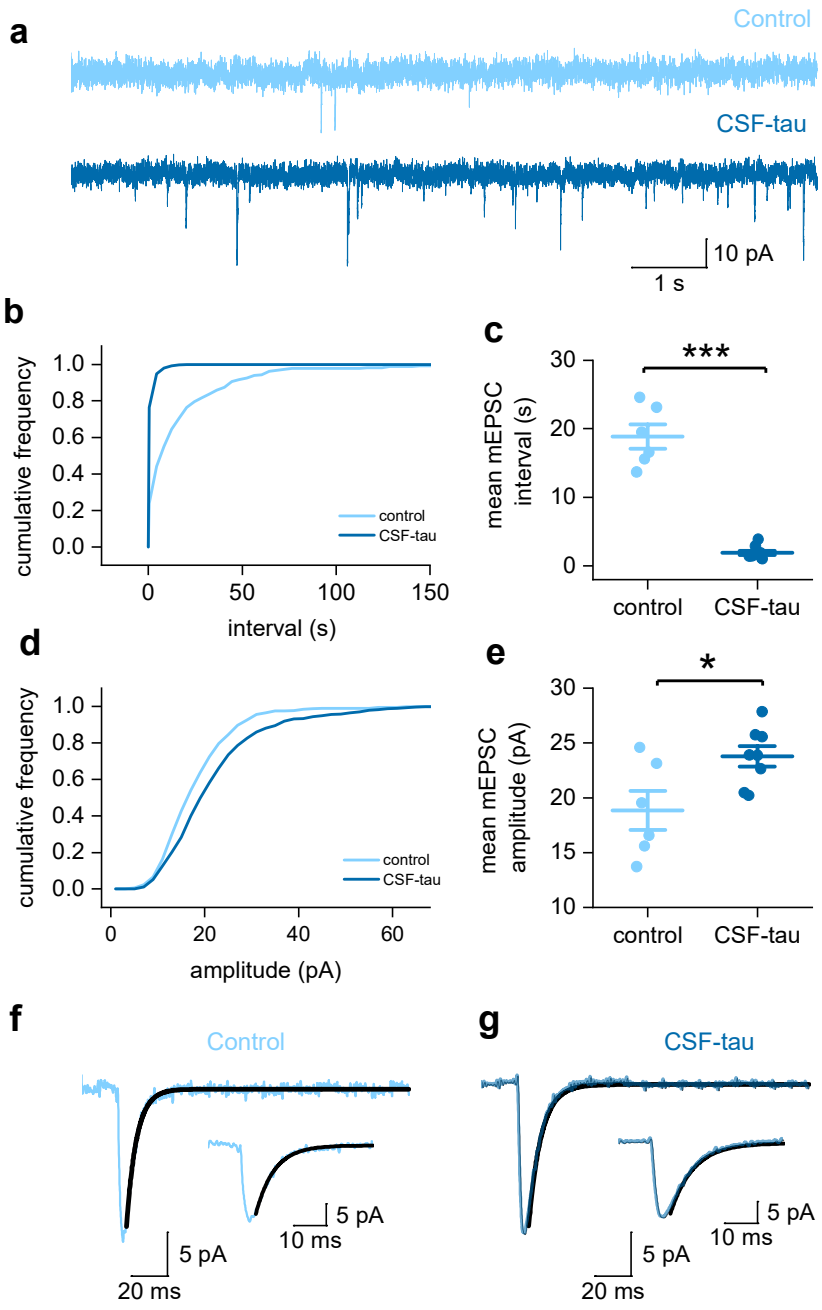

Figure 4: CSF-tau increases the frequency and amplitude of AMPA receptor -mediated mEPSCs. a, Representative traces (10 s duration) from control and CSF-tau incubated slices, demonstrating the significant difference in mEPSC frequency. **b**, Cumulative frequency plot of mEPSC interval (between events). **c,** Mean mEPSC interval for each slice is plotted. CSF-tau decreases the interval between mEPSCs, representing an increase in frequency, compared to control (P=0.0004). **d**, Cumulative frequency plot of mEPSC amplitude. **e**, Mean mEPSC amplitude for each slice is plotted. CSF-tau significantly enhances the amplitude of mEPSCs compared to control (p=0.0426). **f, g**, The average mEPSC waveforms for each recording were analysed for kinetics (10-90% for the rise time and exponential fit for the decay time). An example is shown for control (f) and CSF-tau (g), and the exponential fit is overlaid in black. Inset, higher magnification to show the decay fit. Data is represented as Mean ± SEM.

3.5 CSF-tau alters the generation and maintenance of theta oscillations.

We have found that CSF-tau markedly changes neuronal properties, synaptic transmission, and synaptic plasticity. We have now investigated how these changes can lead to alterations in emergent network activity. Hippocampal hyperexcitability has been identified in AD patients prior to the onset of cognitive symptoms and is associated with increased oscillatory power in theta bands relative to control or MCI groups [45, 64, 89, 90, 98, 109, 111]. Thus, changes in theta power are of interest as a potential predictor for the development of AD [68].

Bath application of the acetylcholine receptor agonist carbachol (50 μM) induced robust, reliable theta oscillations, as demonstrated by Wilcoxon tests comparing peak oscillatory amplitude and baseline activity for all three treatment groups (*Figure 4a-c*). In control slices pre-incubated with aCSF (Figure 4a), there was a significant difference between baseline power and oscillatory power ($W = -138601$, $z = -2.833e-008$, $p < 0.0001$). In slices pre-incubated with CSF-tau (Figure 4b), the difference between baseline power and oscillatory power was also significant ($W = -138601$, $z = -2.830e-007$, $p < 0.0001$). Finally, in slices pre-incubated with CSF-tau-depleted (*Figure 4c*), there was a significant difference between baseline power and oscillatory power ($W = -138601$, $z = -2.214e-008$, $p < 0.0001$). A Kruskal-Wallis test showed that the difference in peak oscillatory power between the three treatment groups was also significant (*Figure 4d*; $H(2) = 166.2$, $p < 0.0001$), with Dunn's tests revealing a significant increase in theta power following CSF-tau treatment relative to aCSF control slices ($p < 0.0001$) and treatment with CSF-tau-depleted ($p < 0.0001$), whilst there was no significant difference between control and CSF-tau-depleted groups. The significant enhancement in the amplitude of hippocampal theta oscillations following incubation with CSF-tau aligns with previous published studies demonstrating that increased theta power is one of the first pathological changes observed in AD patients [14, 32, 36, 69, 89, 91]. Finally, the time to onset of oscillatory activity was also significantly different between groups (*Figure 4e;* $H(2) = 10.09$, $p = 0.0065$), with CSF-tau slices showing a significantly quicker onset of oscillations relative to control ($p = 0.005$) following carbachol application.

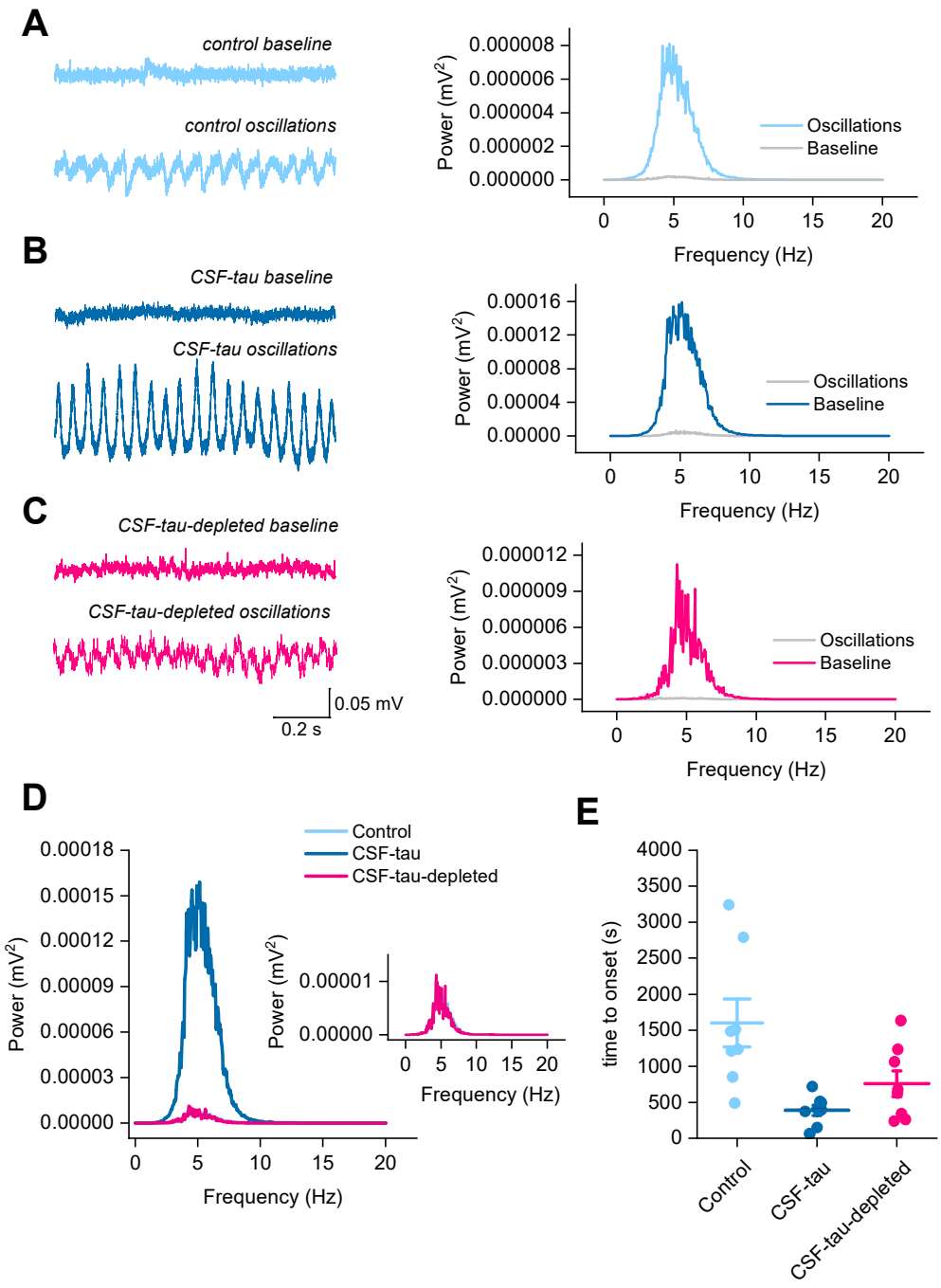

Figure 5. CSF-tau alters the generation and amplitude of theta oscillations. Theta oscillations in the CA3 region of the hippocampus were recorded in an interface chamber (see methods for details). Bath application of carbachol (50 μM) in this study induced robust, reliable theta oscillations across all three experimental conditions (**a, b, c**). **Left,** Representative examples of baseline and theta oscillations for each of the three conditions. **Right,** Power spectrum from the representative example confirming the oscillations to be in the theta range (4-7 Hz). **d,** mean power spectrums for each of the conditions. CSF-tau incubated slices had significantly stronger oscillatory power compared to control or CSF-tau-depleted incubated slices ($P < 0.0001$). Inset, higher magnification of control and CSF-tau-depleted traces. **e,** CSF-tau incubated slices also showed a significantly quicker onset of oscillatory activity relative to control ($p = 0.005$). Data is presented as Mean ± SEM.

4. Discussion

CSF biomarkers for tau and phosphorylated-tau have proved to be reliable predictors/indicators of AD [18, 72]. Tau-based biomarkers can differentiate AD from unaffected individuals and other tauopathies with strong predictive values [72]. Moreover, tau-based biomarker levels change in a stepwise manner across the AD spectrum, allowing for more accurate disease staging, clinical diagnosis, as well as clinical trial recruitment and monitoring [72]. Pathological tau species in AD brains are post-translationally modified, including being phosphorylated and aggregated both in soluble (e.g., oligomers, protomers) and insoluble (neurofibrillary tangles) forms. We currently have high-performing biomarkers that reflect both phosphorylation (e.g., p-tau181) [74] and aggregation [62, 113] of tau in CSF. However, little is known about the toxic effects on brain function of these soluble tau forms in CSF, and this could shed new light on the novel biomarkers developed and applied clinically.

The pathological effects of soluble tau aggregates have been studied extensively in animal models [19, 43, 79, 102, 105]. These changes are normally induced by full-length soluble aggregated forms of tau, mostly produced recombinantly [6, 33, 59, 85]. However, recent work has suggested that tau aggregates produced *in vitro* do not recapitulate the structural features of authentic AD brain tau [132]. We therefore sought to investigate if CSF-tau, which contains high levels of aggregated and non-aggregated tau, often in truncated forms [31], modulates neuronal function.

To do this, we incubated acute mouse brain slices in biomarker-quantified tau-positive CSF pooled from multiple patients. As the goal for future studies is to scale down the volume of sample from pooled samples (5 ml in this study) to individual patient samples (~ 300 μl), to enable correlation with clinical data, we first determined the minimum volume of CSF-tau (diluted in aCSF) for which we could detect a change to neuronal function. We then performed a suite of electrophysiological tests to evaluate the effect on neuronal and network function. We demonstrate that CSF-tau markedly increases neuronal excitability, alters synaptic transmission and plasticity, and modifies the generation and maintenance of hippocampal theta oscillations.

4.1 Immunodepletion of CSF pool to remove tau species.

A wide range of tau fragments can be found in CSF. These are mostly N-terminal to mid-domain tau fragments and provide good biomarkers for disease prognosis, diagnosis, and staging [18, 108]. For this reason, in this study we have used a combination of three antibodies to provide a robust removal of N-term and Mid-terminal tau species: Tau12 N-terminal [epitope = amino acids 6-18], HT7 mid-region [epitope = amino acids 159-163], and TauAB C-terminal antibody [epitope = amino acids 425-441]. To verify the removal of tau after the immuno-depletion, we used different assays that cover various longer (Simoa t-tau assay from Quanterix and p-tau181 [73] and p-tau231 [8] in house assays) and shorter (Lumipulse p-tau181 assay [80]) tau fragments, respectively. Although less abundant, recent studies have shown evidences of other tau fragments in CSF, including microtubule-binding region (MTBR)-containing species [62, 63]. In this initial study, we did not include antibodies specifically targeting the MTBR of tau. Therefore, we cannot guarantee the extent of removal of this region of the protein. However, we demonstrate significant reduction of total and phospho-tau and significant rescue of the

functional effects on neuronal function and oscillations when tau is removed. Thus, the observed changes can be attributed to CSF tau. Additional studies using different antibody panels are nevertheless planned in order to further confirm these results and expand them. While we cannot be certain that all of the observed effects are due solely to tau, as it may exist as a complex with other proteins, we can conclude that, as immuno-depleting for tau abolished the effects, tau must play a central role in mediating the changes.

4.1 CSF-tau led to an increase in excitability and decrease in whole-cell conductance.

We used both standard IV (with step current injections) and the DIVs (with naturalistic current injection) to extract neuronal parameters. In slices incubated with CSF-tau, both approaches for parameterisation measured a marked decrease in whole-cell conductance (rise in neuronal input resistance) and a depolarisation of the resting membrane potential leading to an increase in firing rate (a correlate of neuronal excitability). Obtaining comparable results using two independent methods for the extraction of neuronal parameters strengthens the robustness of this observation.

Depolarisation of the resting membrane potential and neuronal hyperexcitability are consistent with previously reported data in numerous tauopathy models [59, 105, 118, 128], for example in the rTg4510 mouse model, which expresses human tau variant P301L, where the pyramidal cells were depolarised by ~8 mV compared to WT littermates [105]. The increase in input resistance and firing rate, coupled with the observed depolarisation could result from the block of a standing (or leakage) conductance for example a two-pore-domain potassium (K2P) channels that contribute to maintaining the resting potential [84].

A comparable increase in neuronal hyperexcitability has also been observed in AD patients in individuals performing memory-encoding tasks [27, 39, 54]. This phenotype is observed in the early stages of disease, before pronounced cell loss and hypoactivity [12, 46]. Thus, our *in vitro* findings compliment the published literature both for animal models and for early AD when measured in patients [12, 46].

4.2 CSF-tau enhanced synaptic transmission and plasticity.

Soluble tau aggregates have been shown to alter synaptic plasticity both in *in vitro* and *in vivo* models of tauopathy [1, 43, 102, 104]. Therefore, we next investigated if CSF-tau altered synaptic plasticity by measuring LTP. In slices incubated with CSF-tau, we observed enhanced input-output responses. If this was solely due to an increase in release probability, one might expect that there would be less paired pulse facilitation, however, this is not what we observed. Slices incubated with CSF-tau showed significantly enhanced paired pulse facilitation, suggesting that while there may be a change in release probability, there may also be changes in post synaptic receptor numbers and/ or calcium processing.

We then recorded AMPA receptor mediated mEPSCs. In slices incubated with CSF-tau, we observed significant increases in both the amplitude and frequency of mEPSCs. An increase in mEPSC frequency would suggest an increase in release probability, consistent with the increased input-output responses, which could result from an increase in the number of active zones or the number of docked vesicles [9,

97, 131]. The increase in mEPSC amplitude could reflect an increase in the number of postsynaptic receptors, altered vesicle size or an increase in the number of synapses if the mEPSCs are multiquantal [66, 83, 131]. It is also possible that synapses that were previously silent (exhibiting NMDA-receptor mediated synaptic transmission but lacking AMPA receptors) might be unsilenced (via insertion of AMPARs) to give more functional synapses [122]. Silent synapses, which are normally found at the tips of dendritic protrusions called filopodia, allow neurons to maintain more potential for plasticity and have recently been demonstrated to be more abundant in adult mice than once thought [122]. In the rTg4510 tauopathy mouse model, a loss of spine density in the cortex is reported over time and this results from a reduction in mushroom spines. However, in contrast, filopodia are increased [35, 120], suggesting that tau pathology could alter the number of silent synapses and this could contribute to changes in plasticity. In future studies, it would be interesting to examine the ratios of GLUR1 / GLUR2 and also to look at AMPA phosphorylation as phosphorylation of GluA1 at serine 831 and 845 are reported to play key roles in synaptic plasticity [2].

4.3 Alteration to the generation and maintenance of theta oscillations

Functional theta oscillations are dependent upon synchronised activity within the hippocampus, which in turn is mediated by pyramidal cells and interneurons [50]. Parvalbumin (PV)- expressing interneurons are suggested to be particularly critical in regulating pyramidal cell activity [5, 99, 123].

In this study, we have demonstrated that incubation of brain slices with CSF-tau markedly enhanced theta oscillations and increased excitatory pyramidal neuron excitability, and that both of these effects were abolished upon immunodepleting for tau. It is currently unclear whether the increase in excitability of pyramidal cells and changes in glutamatergic transmission are sufficient to produce the observed increases in theta power or whether changes in GABAergic inhibition also occurred. Our findings align with existing data in rodent models and AD patients; the deposition of tau in pyramidal cells and PV interneurons from 1 month of age in 3xTg mice was associated with elevated theta oscillations but no behavioural impairments [88]. The implication that network alterations occur early in the disease course is supported by the oscillatory slowing (an increased power in the theta band) observed in early AD patients accompanied by neuronal hypersynchronisation. Neuronal loss and a global discoordination of network activity then follows in later stages, alongside power alterations in other oscillatory bands such as alpha and delta [22, 41, 42, 52, 53, 76, 95, 96, 101, 106, 115, 116].

This leads to the question of what incubation with CSF-tau in this study might be doing to hippocampal neurons to mediate the elevation in the power of theta oscillations. A combination of experimental and simulated data has indicated that the early-stage AD hyperactivity underpinning oscillatory slowing could be due to pyramidal neuron hyperexcitability [24, 26, 47, 94, 114, 134] and/or reduced excitability of GABAergic PV interneurons and thus pyramidal cell disinhibition [4, 30, 57, 86, 94, 100, 117]. Support for the latter hypothesis of disinhibition also comes from the loss of inhibitory synapses in AD along with the pronounced GABAergic dysfunction observed in AD mouse models, including the model of APOE4, the principal genetic disease risk factor [23, 94]. Such findings provide a potential mechanism for the oscillatory disruption induced by CSF-tau incubation in this study and imply such network alterations to

represent an element of the core, initial neuropathology of AD. Indeed, recent studies are now evaluating the therapeutic implementation of theta entrainment for AD patients [38, 81, 129, 130].

It has also been demonstrated that changes to theta oscillatory power – similar to what we observed herein – can be used to distinguish between prodromal AD and non-AD cases with cognitive decline [94]. The fact that our effects on oscillations agree with clinical human electrophysiological studies gives confidence that this is a method that could, in the future, be clinically useful as in compliment to EEG testing.

4.5 Conclusion

Incubation of acutely-isolated wild-type mouse hippocampal brain slices with small volumes of diluted human CSF-tau allowed us to evaluate effects on neuronal function from single cells through to network level effects. Comparison of the toxicity profiles of the same CSF samples, with and without immuno-depletion for tau, enabled a pioneering demonstration that CSF-tau potently modulates neuronal function. We demonstrate that CSF-tau mediates an increase in neuronal excitability in single cells. We observed, at the network level, increased input-output responses and enhanced paired-pulse facilitation as well as an increase in long-term potentiation. Finally, we show that CSF-tau modifies the generation and maintenance of hippocampal theta oscillations, which have important roles in learning and memory and are known to be altered in AD patients. Together, we describe a novel method for screening human CSF to understand functional effects on neuron and network activity, which could have far-reaching benefits in understanding pathological mechanisms of tauopathies, thus allowing the development of better targeted treatments.

Declarations

Ethics approval and consent to participate.

CSF collection and processing were performed at the University of Gothenburg, Sweden, with local ethical approval, and the samples sent to the University of Warwick, UK, where all experiments were done as approved by the local Human Tissue Authority and Biomedical & Scientific Research Ethics Committees. All animal care and experimental procedures were reviewed and approved by the institutional animal welfare and ethical review body (AWERB) at the University of Warwick.

Consent for publication

All authors have approved the manuscript for submission and that the contents have not been published or submitted elsewhere.

Availability of data and material

The raw data generated and analysed for this manuscript are available from the corresponding author upon reasonable request.

Competing interests

The authors have no conflicts of interest to declare.

Funding

EH holds a Race Against Dementia Fellowship funded by the Barbara Naylor Foundation, in collaboration with ARUK. JB is funded by the Medical Research Council doctoral training partnership at The University of Manchester. AW is funded by the Medical Research Council doctoral training partnership at the University of Warwick. TKK is funded by the Swedish Research Council (Vetenskapsrådet #2021-03244), the Alzheimer's Association Research Fellowship (#AARF-21-850325), the Aina (Ann) Wallströms and Mary-Ann Sjöbloms stiftelsen, and the Emil och Wera Cornells stiftelsen. HZ is a Wallenberg Scholar supported by grants from the Swedish Research Council (#2022-01018), the European Union's Horizon Europe research and innovation programme under grant agreement No 101053962, Swedish State Support for Clinical Research (#ALFGBG-71320), the Alzheimer Drug Discovery Foundation (ADDF), USA (#201809-2016862), the AD Strategic Fund and the Alzheimer's Association (#ADSF-21-831376-C, #ADSF-21-831381-C, and #ADSF-21-831377-C), the Bluefield Project, the Olav Thon Foundation, the Erling-Persson Family Foundation, Stiftelsen för Gamla Tjänarinnor, Hjärnfonden, Sweden (#FO2022-0270), the European Union's Horizon 2020 research and innovation programme under the Marie Skłodowska-Curie grant agreement No 860197 (MIRIADE), the European Union Joint Programme – Neurodegenerative Disease Research (JPND2021-00694), and the UK Dementia Research Institute at UCL (UKDRI-1003). KB is supported by the Swedish Research Council (#2017-00915 and #2022-00732), the Swedish Alzheimer Foundation (#AF-930351, #AF-939721 and #AF-968270), Hjärnfonden, Sweden (#FO2017-0243 and #ALZ2022-0006), the Swedish state under the agreement between the Swedish government and the County Councils, the ALF-agreement (#ALFGBG-715986 and #ALFGBG-965240), the European Union Joint Program for Neurodegenerative Disorders (JPND2019-466-236), the Alzheimer's Association 2021 Zenith Award (ZEN-21-848495), and the Alzheimer's Association 2022-2025 Grant (SG-23-1038904 QC).

Authors' contributions

Conceptualization: **EH, MJW, TKK, JB,** Methodology: **EH, MJW, TKK, JB,** Formal analysis, and Investigation: **EH, MJW, JB, EC, JLR, MO, AW, BM,** Writing - original draft preparation: **EH,** Writing - review and editing: **EH, MJW, TKK, JB, EC, JLR, MO, AW, BM, HZ, KB,** Resources: **EH, MJW, TKK, EC, JLR, MO, HZ, KB,** Supervision: **EH, MJW, TKK**

Acknowledgements

We would like to thank Professor Bruno Frenguelli for providing an interface chamber for the recording of theta oscillations.

References

1. Acquarone E, Argyrousi EK, van den Berg M, Gulisano W, Fà M, Staniszewski A, Calcagno E, Zuccarello E, D'Adamio L, Deng S-X, Puzzo D, Arancio O, Fiorito J (2019) Synaptic and memory dysfunction induced by tau oligomers is rescued by up-regulation of the nitric oxide cascade. Mol Neurodegener 14:26. doi: 10.1186/s13024-019-0326-4

2. Ai H, Yang W, Ye M, Lu W, Yao L, Luo J (2011) Differential regulation of AMPA receptor GluA1 phosphorylation at serine 831 and 845 associated with activation of NMDA receptor subpopulations. Neurosci Lett 497:94–98. doi: 10.1016/j.neulet.2011.04.038

3. Akay M, Wang K, Akay Y, Dragomir A, Wu J (2009) Nonlinear dynamical analysis of carbachol induced hippocampal oscillations in mice | Acta Pharmacologica Sinica

4. Ambrad Giovannetti E, Fuhrmann M (2019) Unsupervised excitation: GABAergic dysfunctions in Alzheimer's disease. Brain Res 1707:216–226. doi: 10.1016/j.brainres.2018.11.042

5. Amilhon B, Huh CYL, Manseau F, Ducharme G, Nichol H, Adamantidis A, Williams S (2015) Parvalbumin Interneurons of Hippocampus Tune Population Activity at Theta Frequency. Neuron 86:1277–1289. doi: 10.1016/j.neuron.2015.05.027

6. Andorfer C, Kress Y, Espinoza M, de Silva R, Tucker KL, Barde Y-A, Duff K, Davies P (2003) Hyperphosphorylation and aggregation of tau in mice expressing normal human tau isoforms. J Neurochem 86:582–590. doi: 10.1046/j.1471-4159.2003.01879.x

7. Apartis E, Poindessous-Jazat FR, Lamour YA, Bassant MH (1998) Loss of Rhythmically Bursting Neurons in Rat Medial Septum Following Selective Lesion of Septohippocampal Cholinergic System. J Neurophysiol 79:1633–1642. doi: 10.1152/jn.1998.79.4.1633

8. Ashton NJ, Pascoal TA, Karikari TK, Benedet AL, Lantero-Rodriguez J, Brinkmalm G, Snellman A, Schöll M, Troakes C, Hye A, Gauthier S, Vanmechelen E, Zetterberg H, Rosa-Neto P, Blennow K (2021) Plasma p-tau231: a new biomarker for incipient Alzheimer's disease pathology. Acta Neuropathol (Berl) 141:709–724. doi: 10.1007/s00401-021-02275-6

9. Auger C, Marty A (2000) Quantal currents at single-site central synapses. J Physiol 526:3–11. doi: 10.1111/j.1469-7793.2000.t01-3-00003.x

10. Badel L, Lefort S, Berger TK, Petersen CCH, Gerstner W, Richardson MJE (2008) Extracting non-linear integrate-and-fire models from experimental data using dynamic I–V curves. Biol Cybern 99:361–370. doi: 10.1007/s00422-008-0259-4

11. Badel L, Lefort S, Brette R, Petersen CCH, Gerstner W, Richardson MJE (2008) Dynamic *I-V* Curves Are Reliable Predictors of Naturalistic Pyramidal-Neuron Voltage Traces. J Neurophysiol 99:656–666. doi: 10.1152/jn.01107.2007

12. Bassett SS, Yousem DM, Cristinzio C, Kusevic I, Yassa MA, Caffo BS, Zeger SL (2006) Familial risk for Alzheimer's disease alters fMRI activation patterns. Brain J Neurol 129:1229–1239. doi: 10.1093/brain/awl089

13. Begus K, Bonawitz E (2020) The rhythm of learning: Theta oscillations as an index of active learning in infancy. Dev Cogn Neurosci 45:100810. doi: 10.1016/j.dcn.2020.100810

14. Bennys K, Rondouin G, Vergnes C, Touchon J (2001) Diagnostic value of quantitative EEG in Alzheimer's disease. Neurophysiol Clin Neurophysiol 31:153–160. doi: 10.1016/S0987-7053(01)00254-4

15. Berry SD, Thompson RF (1978) Prediction of learning rate from the hippocampal electroencephalogram. Science 200:1298–1300. doi: 10.1126/science.663612

16. Bezanson J, Edelman A, Karpinski S, Shah VB (2017) Julia: A Fresh Approach to Numerical Computing. SIAM Rev 59:65–98. doi: 10.1137/141000671

17. Blennow K, Chen C, Cicognola C, Wildsmith KR, Manser PT, Bohorquez SMS, Zhang Z, Xie B, Peng J, Hansson O, Kvartsberg H, Portelius E, Zetterberg H, Lashley T, Brinkmalm G, Kerchner GA, Weimer RM, Ye K, Höglund K (2020) Cerebrospinal fluid tau fragment correlates with tau PET: a candidate biomarker for tangle pathology. Brain 143:650–660. doi: 10.1093/brain/awz346

18. Blennow K, Zetterberg H (2018) Biomarkers for Alzheimer's disease: current status and prospects for the future. J Intern Med 284:643–663. doi: 10.1111/joim.12816

19. Booth CA, Witton J, Nowacki J, Tsaneva-Atanasova K, Jones MW, Randall AD, Brown JT (2016) Altered Intrinsic Pyramidal Neuron Properties and Pathway-Specific Synaptic Dysfunction Underlie Aberrant Hippocampal Network Function in a Mouse Model of Tauopathy. J Neurosci 36:350–363. doi: 10.1523/JNEUROSCI.2151-15.2016

20. Braak H, Braak E (1991) Neuropathological stageing of Alzheimer-related changes. Acta Neuropathol (Berl) 82:239–259. doi: 10.1007/BF00308809

21. Brzezicka A, Kamiński J, Reed CM, Chung JM, Mamelak AN, Rutishauser U (2019) Working Memory Load-related Theta Power Decreases in Dorsolateral Prefrontal Cortex Predict Individual Differences in Performance. J Cogn Neurosci 31:1290–1307. doi: 10.1162/jocn_a_01417

22. Busche MA (2019) Tau suppresses neuronal activity in vivo, even before tangles form. Brain J Neurol 142:843–846. doi: 10.1093/brain/awz060

23. Busche MA, Eichhoff G, Adelsberger H, Abramowski D, Wiederhold K-H, Haass C, Staufenbiel M, Konnerth A, Garaschuk O (2008) Clusters of Hyperactive Neurons Near Amyloid Plaques in a Mouse Model of Alzheimer's Disease. Science 321:1686–1689. doi: 10.1126/science.1162844

24. Busche MA, Konnerth A (2015) Neuronal hyperactivity--A key defect in Alzheimer's disease? BioEssays News Rev Mol Cell Dev Biol 37:624–632. doi: 10.1002/bies.201500004

25. Bush D, Bisby JA, Bird CM, Gollwitzer S, Rodionov R, Diehl B, McEvoy AW, Walker MC, Burgess N (2017) Human hippocampal theta power indicates movement onset and distance travelled. Proc Natl Acad Sci U S A 114:12297–12302. doi: 10.1073/pnas.1708716114

26. Cardin JA, Carlén M, Meletis K, Knoblich U, Zhang F, Deisseroth K, Tsai L-H, Moore CI (2009) Driving fast-spiking cells induces gamma rhythm and controls sensory responses. Nature 459:663–667. doi: 10.1038/nature08002

27. Celone KA, Calhoun VD, Dickerson BC, Atri A, Chua EF, Miller SL, DePeau K, Rentz DM, Selkoe DJ, Blacker D, Albert MS, Sperling RA (2006) Alterations in memory networks in mild cognitive impairment and Alzheimer's disease: an independent component analysis. J Neurosci Off J Soc Neurosci 26:10222–10231. doi: 10.1523/JNEUROSCI.2250-06.2006

28. Chen Z, Mengel D, Keshavan A, Rissman RA, Billinton A, Perkinton M, Percival-Alwyn J, Schultz A, Properzi M, Johnson K, Selkoe DJ, Sperling RA, Patel P, Zetterberg H, Galasko D, Schott JM, Walsh DM (2019) Learnings about the complexity of extracellular tau aid development of a blood-based screen for Alzheimer's disease. Alzheimers Dement J Alzheimers Assoc 15:487–496. doi: 10.1016/j.jalz.2018.09.010

29. Chung DC, Roemer S, Petrucelli L, Dickson DW (2021) Cellular and pathological heterogeneity of primary tauopathies. Mol Neurodegener 16:57. doi: 10.1186/s13024-021-00476-x

30. Chung H, Park K, Jang HJ, Kohl MM, Kwag J (2020) Dissociation of somatostatin and parvalbumin interneurons circuit dysfunctions underlying hippocampal theta and gamma oscillations impaired by amyloid β oligomers in vivo. Brain Struct Funct 225:935–954. doi: 10.1007/s00429-020-02044-3

31. Cicognola C, Brinkmalm G, Wahlgren J, Portelius E, Gobom J, Cullen NC, Hansson O, Parnetti L, Constantinescu R, Wildsmith K, Chen H-H, Beach TG, Lashley T, Zetterberg H, Blennow K, Höglund K (2019) Novel tau fragments in cerebrospinal fluid: relation to tangle pathology and cognitive decline in Alzheimer's disease. Acta Neuropathol (Berl) 137:279–296. doi: 10.1007/s00401-018-1948-2

32. Coben LA, Chi D, Snyder AZ, Storandt M (1990) Replication of a study of frequency analysis of the resting awake EEG in mild probable Alzheimer's disease. Electroencephalogr Clin Neurophysiol 75:148–154. doi: 10.1016/0013-4694(90)90168-j

33. Cowan CM, Chee F, Shepherd D, Mudher A (2010) Disruption of neuronal function by soluble hyperphosphorylated tau in a Drosophila model of tauopathy. Biochem Soc Trans 38:564–570. doi: 10.1042/BST0380564

34. Crespo-García M, Zeiller M, Leupold C, Kreiselmeyer G, Rampp S, Hamer HM, Dalal SS (2016) Slow-theta power decreases during item-place encoding predict spatial accuracy of subsequent context recall. NeuroImage 142:533

35. Crimins JL, Rocher AB, Peters A, Shultz P, Lewis J, Luebke JI (2011) Homeostatic responses by surviving cortical pyramidal cells in neurodegenerative tauopathy. Acta Neuropathol (Berl) 122:551–564. doi: 10.1007/s00401-011-0877-0

36. Czigler B, Csikós D, Hidasi Z, Anna Gaál Z, Csibri E, Kiss E, Salacz P, Molnár M (2008) Quantitative EEG in early Alzheimer's disease patients - power spectrum and complexity features. Int J Psychophysiol Off J Int Organ Psychophysiol 68:75–80. doi: 10.1016/j.ijpsycho.2007.11.002

37. DaSilva LLP, Wall MJ, P de Almeida L, Wauters SC, Januário YC, Müller J, Corrêa SAL (2016) Activity-Regulated Cytoskeleton-Associated Protein Controls AMPAR Endocytosis through a Direct Interaction with Clathrin-Adaptor Protein 2. eNeuro 3:ENEURO.0144-15.2016. doi: 10.1523/ENEURO.0144-15.2016

38. Di Lorenzo F, Bonnì S, Picazio S, Motta C, Caltagirone C, Martorana A, Koch G (2020) Effects of Cerebellar Theta Burst Stimulation on Contralateral Motor Cortex Excitability in Patients with Alzheimer's Disease. Brain Topogr 33:613–617. doi: 10.1007/s10548-020-00781-6

39. Dickerson BC, Salat DH, Greve DN, Chua EF, Rand-Giovannetti E, Rentz DM, Bertram L, Mullin K, Tanzi RE, Blacker D, Albert MS, Sperling RA (2005) Increased hippocampal activation in mild cognitive impairment compared to normal aging and AD. Neurology 65:404–411. doi: 10.1212/01.wnl.0000171450.97464.49

40. Ekstrom AD, Caplan JB, Ho E, Shattuck K, Fried I, Kahana MJ (2005) Human hippocampal theta activity during virtual navigation. Hippocampus 15:881–889. doi: 10.1002/hipo.20109

41. Engels MMA, van der Flier WM, Stam CJ, Hillebrand A, Scheltens P, van Straaten ECW (2017) Alzheimer's disease: The state of the art in resting-state magnetoencephalography. Clin Neurophysiol Off J Int Fed Clin Neurophysiol 128:1426–1437. doi: 10.1016/j.clinph.2017.05.012

42. Engels MMA, Hillebrand A, van der Flier WM, Stam CJ, Scheltens P, van Straaten ECW (2016) Slowing of Hippocampal Activity Correlates with Cognitive Decline in Early Onset Alzheimer's Disease. An MEG Study with Virtual Electrodes. Front Hum Neurosci 10:238. doi: 10.3389/fnhum.2016.00238

43. Fá M, Puzzo D, Piacentini R, Staniszewski A, Zhang H, Baltrons MA, Li Puma DD, Chatterjee I, Li J, Saeed F, Berman HL, Ripoli C, Gulisano W, Gonzalez J, Tian H, Costa JA, Lopez P, Davidowitz E, Yu WH, Haroutunian V, Brown LM, Palmeri A, Sigurdsson EM, Duff KE, Teich AF, Honig LS, Sierks M, Moe JG, D'Adamio L, Grassi C, Kanaan NM, Fraser PE, Arancio O (2016) Extracellular Tau Oligomers Produce An Immediate Impairment of LTP and Memory. Sci Rep 6:19393. doi: 10.1038/srep19393

44. Fellous J-M, Sejnowski TJ (2000) Cholinergic induction of oscillations in the hippocampal slice in the slow (0.5–2 Hz), theta (5–12 Hz), and gamma (35–70 Hz) bands. Hippocampus 10:187–197. doi: 10.1002/(SICI)1098-1063(2000)10:2<187::AID-HIPO8>3.0.CO;2-M

45. Fernández A, Maestú F, Amo C, Gil P, Fehr T, Wienbruch C, Rockstroh B, Elbert T, Ortiz T (2002) Focal temporoparietal slow activity in Alzheimer's disease revealed by magnetoencephalography. Biol Psychiatry 52:764–770. doi: 10.1016/S0006-3223(02)01366-5

46. Filippini N, MacIntosh BJ, Hough MG, Goodwin GM, Frisoni GB, Smith SM, Matthews PM, Beckmann CF, Mackay CE (2009) Distinct patterns of brain activity in young carriers of the APOE-epsilon4 allele. Proc Natl Acad Sci U S A 106:7209–7214. doi: 10.1073/pnas.0811879106

47. Ghatak S, Dolatabadi N, Trudler D, Zhang X, Wu Y, Mohata M, Ambasudhan R, Talantova M, Lipton SA (2019) Mechanisms of hyperexcitability in Alzheimer's disease hiPSC-derived neurons and cerebral organoids vs isogenic controls. eLife 8:e50333. doi: 10.7554/eLife.50333

48. Gobom J, Benedet AL, Mattsson-Carlgren N, Montoliu-Gaya L, Schultz N, Ashton NJ, Janelidze S, Servaes S, Sauer M, Pascoal TA, Karikari TK, Lantero-Rodriguez J, Brinkmalm G, Zetterberg H, Hansson O, Rosa-Neto P, Blennow K (2022) Antibody-free measurement of cerebrospinal fluid tau phosphorylation across the Alzheimer's disease continuum. Mol Neurodegener 17:81. doi: 10.1186/s13024-022-00586-0

49. Gobom J, Parnetti L, Rosa-Neto P, Vyhnalek M, Gauthier S, Cataldi S, Lerch O, Laczo J, Cechova K, Clarin M, Benet AL, Pascoal TA, Rahmouni N, Vandijck M, Huyck E, Bastard NL, Stevenson J, Chamoun M, Alcolea D, Lleó A, Andreasson U, Verbeek MM, Bellomo G, Rinaldi R, Ashton NJ, Zetterberg H, Sheardova K, Hort J, Blennow K (2022) Validation of the LUMIPULSE automated immunoassay for the measurement of core AD biomarkers in cerebrospinal fluid. Clin Chem Lab Med CCLM 60:207–219. doi: 10.1515/cclm-2021-0651

50. Goutagny R, Jackson J, Williams S (2009) Self-generated theta oscillations in the hippocampus. Nat Neurosci 12:1491–1493. doi: 10.1038/nn.2440

51. Goutagny R, Krantic S (2013) Hippocampal Oscillatory Activity in Alzheimer's Disease: Toward the Identification of Early Biomarkers? Aging Dis 4:134–140

52. Haan W de, Mott K, Straaten ECW van, Scheltens P, Stam CJ (2012) Activity Dependent Degeneration Explains Hub Vulnerability in Alzheimer's Disease. PLOS Comput Biol 8:e1002582. doi: 10.1371/journal.pcbi.1002582

53. de Haan W, Stam CJ, Jones BF, Zuiderwijk IM, van Dijk BW, Scheltens P (2008) Resting-state oscillatory brain dynamics in Alzheimer disease. J Clin Neurophysiol Off Publ Am Electroencephalogr Soc 25:187–193. doi: 10.1097/WNP.0b013e31817da184

54. Hämäläinen A, Pihlajamäki M, Tanila H, Hänninen T, Niskanen E, Tervo S, Karjalainen PA, Vanninen RL, Soininen H (2007) Increased fMRI responses during encoding in mild cognitive impairment. Neurobiol Aging 28:1889–1903. doi: 10.1016/j.neurobiolaging.2006.08.008

55. Han P, Serrano G, Beach TG, Caselli RJ, Yin J, Zhuang N, Shi J (2017) A Quantitative Analysis of Brain Soluble Tau and the Tau Secretion Factor. J Neuropathol Exp Neurol 76:44–51. doi: 10.1093/jnen/nlw105

56. Harrison PM, Badel L, Wall MJ, Richardson MJE (2015) Experimentally Verified Parameter Sets for Modelling Heterogeneous Neocortical Pyramidal-Cell Populations. PLOS Comput Biol 11:e1004165. doi: 10.1371/journal.pcbi.1004165

57. Hijazi S, Heistek TS, Scheltens P, Neumann U, Shimshek DR, Mansvelder HD, Smit AB, van Kesteren RE (2020) Early restoration of parvalbumin interneuron activity prevents memory loss and network hyperexcitability in a mouse model of Alzheimer's disease. Mol Psychiatry 25:3380–3398. doi: 10.1038/s41380-019-0483-4

58. Hill E, Karikari TK, Lantero-Rodriguez J, Zetterberg H, Blennow K, Richardson MJ, Wall MJ (2021) Truncating tau reveals different pathophysiological actions of oligomers in single neurons. Commun Biol 4:1265. doi: 10.1038/s42003-021-02791-x

59. Hill E, Karikari TK, Moffat KG, Richardson MJE, Wall MJ (2019) Introduction of Tau Oligomers into Cortical Neurons Alters Action Potential Dynamics and Disrupts Synaptic Transmission and Plasticity. eneuro 6:ENEURO.0166-19.2019. doi: 10.1523/ENEURO.0166-19.2019

60. Hill E, Wall MJ, Moffat KG, Karikari TK (2020) Understanding the Pathophysiological Actions of Tau Oligomers: A Critical Review of Current Electrophysiological Approaches. Front Mol Neurosci 13. doi: 10.3389/fnmol.2020.00155

61. Hölscher C, McGlinchey L, Anwyl R, Rowan MJ (1997) HFS-induced long-term potentiation and LFS-induced depotentiation in area CA1 of the hippocampus are not good models for learning. Psychopharmacology (Berl) 130:174–182. doi: 10.1007/s002130050226

62. Horie K, Barthélemy NR, Sato C, Bateman RJ (2020) CSF tau microtubule binding region identifies tau tangle and clinical stages of Alzheimer's disease. Brain 144:515–527. doi: 10.1093/brain/awaa373

63. Horie K, Barthélemy NR, Spina S, VandeVrede L, He Y, Paterson RW, Wright BA, Day GS, Davis AA, Karch CM, Seeley WW, Perrin RJ, Koppisetti RK, Shaikh F, Lago AL, Heuer HW, Ghoshal N, Gabelle A, Miller BL, Boxer AL, Bateman RJ, Sato C (2022) CSF tau microtubule-binding region identifies pathological changes in primary tauopathies. Nat Med 28:2547–2554. doi: 10.1038/s41591-022-02075-9

64. Hsiao F-J, Wang Y-J, Yan S-H, Chen W-T, Lin Y-Y (2013) Altered Oscillation and Synchronization of Default-Mode Network Activity in Mild Alzheimer's Disease Compared to Mild

Cognitive Impairment: An Electrophysiological Study. PLOS ONE 8:e68792. doi: 10.1371/journal.pone.0068792

65. Ishida K, Yamada K, Nishiyama R, Hashimoto T, Nishida I, Abe Y, Yasui M, Iwatsubo T (2022) Glymphatic system clears extracellular tau and protects from tau aggregation and neurodegeneration. J Exp Med 219:e20211275. doi: 10.1084/jem.20211275

66. Ishikawa T, Sahara Y, Takahashi T (2002) A Single Packet of Transmitter Does Not Saturate Postsynaptic Glutamate Receptors. Neuron 34:613–621. doi: 10.1016/S0896-6273(02)00692-X

67. Jack CR, Bennett DA, Blennow K, Carrillo MC, Dunn B, Haeberlein SB, Holtzman DM, Jagust W, Jessen F, Karlawish J, Liu E, Molinuevo JL, Montine T, Phelps C, Rankin KP, Rowe CC, Scheltens P, Siemers E, Snyder HM, Sperling R, Contributors (2018) NIA-AA Research Framework: Toward a biological definition of Alzheimer's disease. Alzheimers Dement J Alzheimers Assoc 14:535–562. doi: 10.1016/j.jalz.2018.02.018

68. Jelic V, Johansson SE, Almkvist O, Shigeta M, Julin P, Nordberg A, Winblad B, Wahlund LO (2000) Quantitative electroencephalography in mild cognitive impairment: longitudinal changes and possible prediction of Alzheimer's disease. Neurobiol Aging 21:533–540. doi: 10.1016/s0197-4580(00)00153-6

69. Jeong J (2004) EEG dynamics in patients with Alzheimer's disease. Clin Neurophysiol Off J Int Fed Clin Neurophysiol 115:1490–1505. doi: 10.1016/j.clinph.2004.01.001

70. Jin Y, Su Q-X, Shen J-X, Marks MJ, Wu J (2013) Impaired Hippocampal Theta Oscillations in the Mice Null Alpha7 Nicotinic Acetylcholine Receptors. CNS Neurosci Ther 19:721–723. doi: 10.1111/cns.12138

71. Kanmert D, Cantlon A, Muratore CR, Jin M, O'Malley TT, Lee G, Young-Pearse TL, Selkoe DJ, Walsh DM (2015) C-Terminally Truncated Forms of Tau, But Not Full-Length Tau or Its C-Terminal Fragments, Are Released from Neurons Independently of Cell Death. J Neurosci 35:10851–10865. doi: 10.1523/JNEUROSCI.0387-15.2015

72. Karikari TK, Ashton NJ, Brinkmalm G, Brum WS, Benedet AL, Montoliu-Gaya L, Lantero-Rodriguez J, Pascoal TA, Suárez-Calvet M, Rosa-Neto P, Blennow K, Zetterberg H (2022) Blood phospho-tau in Alzheimer disease: analysis, interpretation, and clinical utility. Nat Rev Neurol 18:400–418. doi: 10.1038/s41582-022-00665-2

73. Karikari TK, Benedet AL, Ashton NJ, Lantero Rodriguez J, Snellman A, Suárez-Calvet M, Saha-Chaudhuri P, Lussier F, Kvartsberg H, Rial AM, Pascoal TA, Andreasson U, Schöll M, Weiner MW, Rosa-Neto P, Trojanowski JQ, Shaw LM, Blennow K, Zetterberg H, Alzheimer's Disease Neuroimaging Initiative (2021) Diagnostic performance and prediction of clinical progression of plasma phospho-tau181 in the Alzheimer's Disease Neuroimaging Initiative. Mol Psychiatry 26:429–442. doi: 10.1038/s41380-020-00923-z

74. Karikari TK, Pascoal TA, Ashton NJ, Janelidze S, Benedet AL, Rodriguez JL, Chamoun M, Savard M, Kang MS, Therriault J, Schöll M, Massarweh G, Soucy J-P, Höglund K, Brinkmalm G, Mattsson N, Palmqvist S, Gauthier S, Stomrud E, Zetterberg H, Hansson O, Rosa-Neto P, Blennow K (2020) Blood phosphorylated tau 181 as a biomarker for Alzheimer's disease: a diagnostic performance and prediction modelling study using data from four prospective cohorts. Lancet Neurol 19:422–433. doi: 10.1016/S1474-4422(20)30071-5

75. Kim S-P, Kang J-H, Choe S-H, Jeong JW, Kim HT, Yun K, Jeong J, Lee S-H (2012) Modulation of theta phase synchronization in the human electroencephalogram during a recognition memory task. Neuroreport 23:637–641. doi: 10.1097/WNR.0b013e328354afed

76. Koelewijn L, Lancaster TM, Linden D, Dima DC, Routley BC, Magazzini L, Barawi K, Brindley L, Adams R, Tansey KE, Bompas A, Tales A, Bayer A, Singh K (2019) Oscillatory hyperactivity and hyperconnectivity in young APOE-ε4 carriers and hypoconnectivity in Alzheimer's disease. eLife 8:e36011. doi: 10.7554/eLife.36011

77. Lantero-Rodriguez J, Snellman A, Benedet AL, Milà-Alomà M, Camporesi E, Montoliu-Gaya L, Ashton NJ, Vrillon A, Karikari TK, Gispert JD, Salvadó G, Shekari M, Toomey CE, Lashley TL, Zetterberg H, Suárez-Calvet M, Brinkmalm G, Rosa Neto P, Blennow K (2021) P-tau235: a novel biomarker for staging preclinical Alzheimer's disease. EMBO Mol Med 13:e15098. doi: 10.15252/emmm.202115098

78. Lasagna-Reeves CA, Castillo-Carranza DL, Sengupta U, Guerrero-Munoz MJ, Kiritoshi T, Neugebauer V, Jackson GR, Kayed R (2012) Alzheimer brain-derived tau oligomers propagate pathology from endogenous tau. Sci Rep 2:700. doi: 10.1038/srep00700

79. Lasagna-Reeves CA, Castillo-Carranza DL, Sengupta U, Sarmiento J, Troncoso J, Jackson GR, Kayed R (2012) Identification of oligomers at early stages of tau aggregation in Alzheimer's disease. FASEB J Off Publ Fed Am Soc Exp Biol 26:1946–1959. doi: 10.1096/fj.11-199851

80. Leitão MJ, Silva-Spínola A, Santana I, Olmedo V, Nadal A, Le Bastard N, Baldeiras I (2019) Clinical validation of the Lumipulse G cerebrospinal fluid assays for routine diagnosis of Alzheimer's disease. Alzheimers Res Ther 11:91. doi: 10.1186/s13195-019-0550-8

81. Li G, Bien-Ly N, Andrews-Zwilling Y, Xu Q, Bernardo A, Ring K, Halabisky B, Deng C, Mahley RW, Huang Y (2009) GABAergic interneuron dysfunction impairs hippocampal neurogenesis in adult apolipoprotein E4 knockin mice. Cell Stem Cell 5:634–645. doi: 10.1016/j.stem.2009.10.015

82. Lisman JE, Jensen O (2013) The θ-γ neural code. Neuron 77:1002–1016. doi: 10.1016/j.neuron.2013.03.007

83. Liu G, Choi S, Tsien RW (1999) Variability of Neurotransmitter Concentration and Nonsaturation of Postsynaptic AMPA Receptors at Synapses in Hippocampal Cultures and Slices. Neuron 22:395–409. doi: 10.1016/S0896-6273(00)81099-5

84. Luo Y, Huang L, Liao P, Jiang R (2021) Contribution of Neuronal and Glial Two-Pore-Domain Potassium Channels in Health and Neurological Disorders. Neural Plast 2021:8643129. doi: 10.1155/2021/8643129

85. Maeda S, Sahara N, Saito Y, Murayama S, Ikai A, Takashima A (2006) Increased levels of granular tau oligomers: an early sign of brain aging and Alzheimer's disease. Neurosci Res 54:197–201. doi: 10.1016/j.neures.2005.11.009

86. Martinez-Losa M, Tracy TE, Ma K, Verret L, Clemente-Perez A, Khan AS, Cobos I, Ho K, Gan L, Mucke L, Alvarez-Dolado M, Palop JJ (2018) Nav1.1-Overexpressing Interneuron Transplants Restore Brain Rhythms and Cognition in a Mouse Model of Alzheimer's Disease. Neuron 98:75-89.e5. doi: 10.1016/j.neuron.2018.02.029

87. Meredith Jr JE, Sankaranarayanan S, Guss V, Lanzetti AJ, Berisha F, Neely RJ, Slemmon JR, Portelius E, Zetterberg H, Blennow K, Soares H, Ahlijanian M, Albright CF (2013) Characterization of

Novel CSF Tau and ptau Biomarkers for Alzheimer's Disease. PLOS ONE 8:e76523. doi: 10.1371/journal.pone.0076523

88. Mondragón-Rodríguez S, Salas-Gallardo A, González-Pereyra P, Macías M, Ordaz B, Peña-Ortega F, Aguilar-Vázquez A, Orta-Salazar E, Díaz-Cintra S, Perry G, Williams S (2018) Phosphorylation of Tau protein correlates with changes in hippocampal theta oscillations and reduces hippocampal excitability in Alzheimer's model. J Biol Chem 293:8462–8472. doi: 10.1074/jbc.RA117.001187

89. Moretti DV, Babiloni C, Binetti G, Cassetta E, Dal Forno G, Ferreric F, Ferri R, Lanuzza B, Miniussi C, Nobili F, Rodriguez G, Salinari S, Rossini PM (2004) Individual analysis of EEG frequency and band power in mild Alzheimer's disease. Clin Neurophysiol 115:299–308. doi: 10.1016/S1388-2457(03)00345-6

90. Mormino E, Brandel M, Madison C, Marks S, Baker S, Jagust WJ (2011) Aβ Deposition in Aging Is Associated with Increases in Brain Activation during Successful Memory Encoding | Cerebral Cortex | Oxford Academic

91. Musaeus CS, Engedal K, Høgh P, Jelic V, Mørup M, Naik M, Oeksengaard A-R, Snaedal J, Wahlund L-O, Waldemar G, Andersen BB (2018) EEG Theta Power Is an Early Marker of Cognitive Decline in Dementia due to Alzheimer's Disease. J Alzheimers Dis JAD 64:1359–1371. doi: 10.3233/JAD-180300

92. Nelson PT, Alafuzoff I, Bigio EH, Bouras C, Braak H, Cairns NJ, Castellani RJ, Crain BJ, Davies P, Del Tredici K, Duyckaerts C, Frosch MP, Haroutunian V, Hof PR, Hulette CM, Hyman BT, Iwatsubo T, Jellinger KA, Jicha GA, Kövari E, Kukull WA, Leverenz JB, Love S, Mackenzie IR, Mann DM, Masliah E, McKee AC, Montine TJ, Morris JC, Schneider JA, Sonnen JA, Thal DR, Trojanowski JQ, Troncoso JC, Wisniewski T, Woltjer RL, Beach TG (2012) Correlation of Alzheimer Disease Neuropathologic Changes With Cognitive Status: A Review of the Literature. J Neuropathol Exp Neurol 71:362–381. doi: 10.1097/NEN.0b013e31825018f7

93. Niewiadomska G, Niewiadomski W, Steczkowska M, Gasiorowska A (2021) Tau Oligomers Neurotoxicity. Life 11:28. doi: 10.3390/life11010028

94. van Nifterick AM, Gouw AA, van Kesteren RE, Scheltens P, Stam CJ, de Haan W (2022) A multiscale brain network model links Alzheimer's disease-mediated neuronal hyperactivity to large-scale oscillatory slowing. Alzheimers Res Ther 14:101. doi: 10.1186/s13195-022-01041-4

95. Ochoa JF, Alonso JF, Duque JE, Tobón CA, Baena A, Lopera F, Mañanas MA, Hernández AM (2017) Precuneus Failures in Subjects of the PSEN1 E280A Family at Risk of Developing Alzheimer's Disease Detected Using Quantitative Electroencephalography. J Alzheimer39s Dis 58:1229

96. Ochoa JF, Alonso JF, Duque JE, Tobón CA, Mañanas MA, Lopera F, Hernández AM Successful Object Encoding Induces Increased Directed Connectivity in Presymptomatic Early-Onset Alzheimer's Disease. J Alzheimers Dis 55:1195–1205. doi: 10.3233/JAD-160803

97. Oertner TG, Sabatini BL, Nimchinsky EA, Svoboda K (2002) Facilitation at single synapses probed with optical quantal analysis. Nat Neurosci 5:657–664. doi: 10.1038/nn867

98. Osipova D, Ahveninen J, Jensen O, Ylikoski A, Pekkonen E (2005) Altered generation of spontaneous oscillations in Alzheimer's disease. NeuroImage 27:835–841. doi: 10.1016/j.neuroimage.2005.05.011

99. Palop JJ, Chin J, Roberson ED, Wang J, Thwin MT, Bien-Ly N, Yoo J, Ho KO, Yu G-Q, Kreitzer A, Finkbeiner S, Noebels JL, Mucke L (2007) Aberrant excitatory neuronal activity and compensatory remodeling of inhibitory hippocampal circuits in mouse models of Alzheimer's disease. Neuron 55:697–711. doi: 10.1016/j.neuron.2007.07.025

100. Palop JJ, Mucke L (2016) Network abnormalities and interneuron dysfunction in Alzheimer disease. Nat Rev Neurosci 17:777–792. doi: 10.1038/nrn.2016.141

101. Pusil S, López ME, Cuesta P, Bruña R, Pereda E, Maestú F (2019) Hypersynchronization in mild cognitive impairment: the "X" model. Brain J Neurol 142:3936–3950. doi: 10.1093/brain/awz320

102. Puzzo D, Piacentini R, Fá M, Gulisano W, Li Puma DD, Staniszewski A, Zhang H, Tropea MR, Cocco S, Palmeri A, Fraser P, D'Adamio L, Grassi C, Arancio O (2017) LTP and memory impairment caused by extracellular Aβ and Tau oligomers is APP-dependent. eLife 6. doi: 10.7554/eLife.26991

103. Raghavachari S, Kahana MJ, Rizzuto DS, Caplan JB, Kirschen MP, Bourgeois B, Madsen JR, Lisman JE (2001) Gating of human theta oscillations by a working memory task. J Neurosci Off J Soc Neurosci 21:3175–3183. doi: 10.1523/JNEUROSCI.21-09-03175.2001

104. Regan P, Piers T, Yi J-H, Kim D-H, Huh S, Park SJ, Ryu JH, Whitcomb DJ, Cho K (2015) Tau phosphorylation at serine 396 residue is required for hippocampal LTD. J Neurosci Off J Soc Neurosci 35:4804–4812. doi: 10.1523/JNEUROSCI.2842-14.2015

105. Rocher AB, Crimins JL, Amatrudo JM, Kinson MS, Todd-Brown MA, Lewis J, Luebke JI (2010) Structural and functional changes in tau mutant mice neurons are not linked to the presence of NFTs. Exp Neurol 223:385–393. doi: 10.1016/j.expneurol.2009.07.029

106. Rodriguez GA, Barrett GM, Duff KE, Hussaini SA (2020) Chemogenetic attenuation of neuronal activity in the entorhinal cortex reduces Aβ and tau pathology in the hippocampus. PLOS Biol 18:e3000851. doi: 10.1371/journal.pbio.3000851

107. Sato C, Barthélemy NR, Mawuenyega KG, Patterson BW, Gordon BA, Jockel-Balsarotti J, Sullivan M, Crisp MJ, Kasten T, Kirmess KM, Kanaan NM, Yarasheski KE, Baker-Nigh A, Benzinger TLS, Miller TM, Karch CM, Bateman RJ (2018) Tau Kinetics in Neurons and the Human Central Nervous System. Neuron 97:1284-1298.e7. doi: 10.1016/j.neuron.2018.02.015

108. Scheltens P, Blennow K, Breteler MMB, de Strooper B, Frisoni GB, Salloway S, Van der Flier WM (2016) Alzheimer's disease. Lancet Lond Engl 388:505–517. doi: 10.1016/S0140-6736(15)01124-1

109. Schreiter-Gasser U, Gasser T, Ziegler P (1994) Quantitative EEG analysis in early onset Alzheimer's disease: correlations with severity, clinical characteristics, visual EEG and CCT. Electroencephalogr Clin Neurophysiol 90:267–272. doi: 10.1016/0013-4694(94)90144-9

110. Serrano-Pozo A, Frosch MP, Masliah E, Hyman BT (2011) Neuropathological alterations in Alzheimer disease. Cold Spring Harb Perspect Med 1:a006189. doi: 10.1101/cshperspect.a006189

111. Setti SE, Hunsberger HC, Reed MN (2017) Alterations in hippocampal activity and Alzheimer's disease. Transl Issues Psychol Sci 3:348–356. doi: 10.1037/tps0000124

112. Shafiei SS, Guerrero-Muñoz MJ, Castillo-Carranza DL (2017) Tau Oligomers: Cytotoxicity, Propagation, and Mitochondrial Damage. Front Aging Neurosci 9

113. Simrén J, Brum WS, Ashton NJ, Benedet AL, Karikari TK, Kvartsberg H, Sjons E, Lussier FZ, Chamoun M, Stevenson J, Hopewell R, Pallen V, Ye K, Pascoal TA, Zetterberg H, Rosa-Neto P, Blennow K (2022) CSF tau368/total-tau ratio reflects cognitive performance and neocortical tau better compared to p-tau181 and p-tau217 in cognitively impaired individuals. Alzheimers Res Ther 14:192. doi: 10.1186/s13195-022-01142-0

114. Sohal VS, Zhang F, Yizhar O, Deisseroth K (2009) Parvalbumin neurons and gamma rhythms enhance cortical circuit performance. Nature 459:698–702. doi: 10.1038/nature07991

115. Sperling RA, Dickerson BC, Pihlajamaki M, Vannini P, LaViolette PS, Vitolo OV, Hedden T, Becker JA, Rentz DM, Selkoe DJ, Johnson KA (2010) Functional Alterations in Memory Networks in Early Alzheimer's Disease. Neuromolecular Med 12:27–43. doi: 10.1007/s12017-009-8109-7

116. Stam CJ, de Haan W, Daffertshofer A, Jones BF, Manshanden I, van Cappellen van Walsum AM, Montez T, Verbunt JPA, de Munck JC, van Dijk BW, Berendse HW, Scheltens P (2009) Graph theoretical analysis of magnetoencephalographic functional connectivity in Alzheimer's disease. Brain J Neurol 132:213–224. doi: 10.1093/brain/awn262

117. Stefanovski L, Triebkorn P, Spiegler A, Diaz-Cortes M-A, Solodkin A, Jirsa V, McIntosh AR, Ritter P, Alzheimer's Disease Neuroimaging Initiative (2019) Linking Molecular Pathways and Large-Scale Computational Modeling to Assess Candidate Disease Mechanisms and Pharmacodynamics in Alzheimer's Disease. Front Comput Neurosci 13:54. doi: 10.3389/fncom.2019.00054

118. Targa Dias Anastacio H, Matosin N, Ooi L (2022) Neuronal hyperexcitability in Alzheimer's disease: what are the drivers behind this aberrant phenotype? Transl Psychiatry 12:1–14. doi: 10.1038/s41398-022-02024-7

119. Teles-Grilo Ruivo LM, Mellor JR (2013) Cholinergic modulation of hippocampal network function. Front Synaptic Neurosci 5:2. doi: 10.3389/fnsyn.2013.00002

120. Tracy TE, Gan L (2018) Tau-mediated synaptic and neuronal dysfunction in neurodegenerative disease. Curr Opin Neurobiol 51:134–138. doi: 10.1016/j.conb.2018.04.027

121. Uhlenbeck GE, Ornstein LS (1930) On the Theory of the Brownian Motion. Phys Rev 36:823–841. doi: 10.1103/PhysRev.36.823

122. Vardalaki D, Chung K, Harnett MT (2022) Filopodia are a structural substrate for silent synapses in adult neocortex. Nature 612:323–327. doi: 10.1038/s41586-022-05483-6

123. Verret L, Mann EO, Hang GB, Barth AMI, Cobos I, Ho K, Devidze N, Masliah E, Kreitzer AC, Mody I, Mucke L, Palop JJ (2012) Inhibitory interneuron deficit links altered network activity and cognitive dysfunction in Alzheimer model. Cell 149:708–721. doi: 10.1016/j.cell.2012.02.046

124. Vertes RP, Hoover WB, Viana Di Prisco G (2004) Theta rhythm of the hippocampus: subcortical control and functional significance. Behav Cogn Neurosci Rev 3:173–200. doi: 10.1177/1534582304273594

125. Ward SM, Himmelstein DS, Lancia JK, Binder LI (2012) Tau oligomers and tau toxicity in neurodegenerative disease. Biochem Soc Trans 40:667–671. doi: 10.1042/BST20120134

126. Williams JH, Kauer JA (1997) Properties of Carbachol-Induced Oscillatory Activity in Rat Hippocampus. J Neurophysiol 78:2631–2640. doi: 10.1152/jn.1997.78.5.2631

127. Winson J (1978) Loss of hippocampal theta rhythm results in spatial memory deficit in the rat. Science 201:160–163. doi: 10.1126/science.663646

128. Witton J, Staniaszek LE, Bartsch U, Randall AD, Jones MW, Brown JT (2016) Disrupted hippocampal sharp-wave ripple-associated spike dynamics in a transgenic mouse model of dementia. J Physiol 594:4615–4630. doi: 10.1113/jphysiol.2014.282889

129. Wu X, Ji G-J, Geng Z, Wang L, Yan Y, Wu Y, Xiao G, Gao L, Wei Q, Zhou S, Wei L, Tian Y, Wang K (2022) Accelerated intermittent theta-burst stimulation broadly ameliorates symptoms and cognition in Alzheimer's disease: A randomized controlled trial. Brain Stimulat 15:35–45. doi: 10.1016/j.brs.2021.11.007

130. Wu X, Ji G-J, Geng Z, Zhou S, Yan Y, Wei L, Qiu B, Tian Y, Wang K (2020) Strengthened theta-burst transcranial magnetic stimulation as an adjunctive treatment for Alzheimer's disease: An open-label pilot study. Brain Stimulat 13:484–486. doi: 10.1016/j.brs.2019.12.020

131. Zhang J, Yang Y, Li H, Cao J, Xu L (2005) Amplitude/frequency of spontaneous mEPSC correlates to the degree of long-term depression in the CA1 region of the hippocampal slice. Brain Res 1050:110–117. doi: 10.1016/j.brainres.2005.05.032

132. Zhang W, Falcon B, Murzin AG, Fan J, Crowther RA, Goedert M, Scheres SH (2019) Heparin-induced tau filaments are polymorphic and differ from those in Alzheimer's and Pick's diseases. eLife 8:e43584. doi: 10.7554/eLife.43584

133. Zhu G, Liu Y, Wang Y, Bi X, Baudry M (2015) Different Patterns of Electrical Activity Lead to Long-term Potentiation by Activating Different Intracellular Pathways. J Neurosci 35:621–633. doi: 10.1523/JNEUROSCI.2193-14.2015

134. Zott B, Simon MM, Hong W, Unger F, Chen-Engerer H-J, Frosch MP, Sakmann B, Walsh DM, Konnerth A (2019) A vicious cycle of β amyloid-dependent neuronal hyperactivation. Science 365:559–565. doi: 10.1126/science.aay0198

Supplementary material

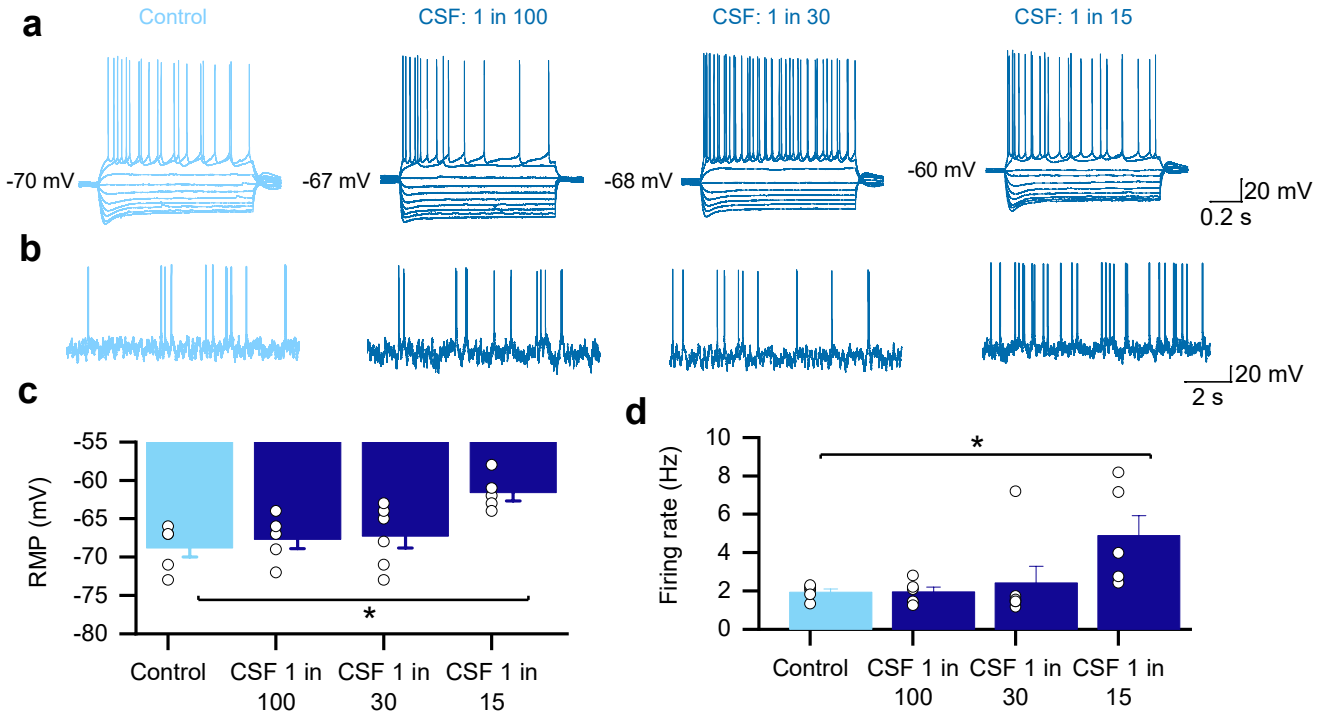

Supplementary figure 1. We diluted the CSF-tau sample with artificial CSF (aCSF) to reduce the volume of sample that was used for each experiment. As the end goal will be to use individual patient samples (much smaller volumes ~300 µl) to enable correlation with clinical data, we first sought to find the minimum volume (maximum dilution in aCSF) of CSF-tau, for which we could detect a change in neuronal function. Representative examples of standard current-voltage responses for slices that have been incubated in control aCSF vs different dilutions of CSF in aCSF (1:100, 1:30 and 1:15 dilutions). Using neuronal excitability, measured using whole-cell patch clamp recording from single CA1 pyramidal cells in the hippocampus as a readout. We found no significant changes to neuronal excitability with either 1:100 dilution or 1:30 dilution of CSF-tau, but a significant depolarisation (**a**; p = 0.0212) and increase in firing rate (**b**; p=0.0215) was observed with a 1:15 dilution (100 µl CSF in 1.5 ml aCSF) compared to control slices.

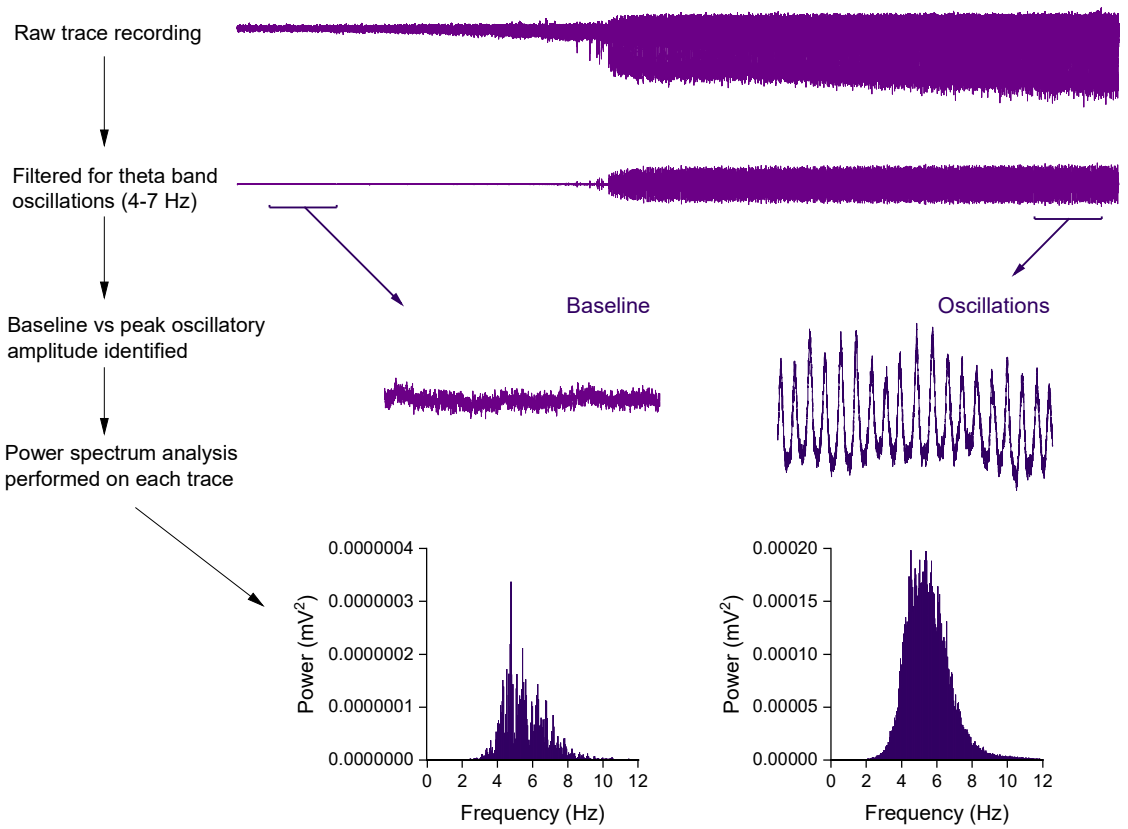

Supplementary figure 2 – Protocol for analysis of hippocampal CA3 theta oscillations. Carbachol-elicited oscillations were characterised using power spectral density (PSD) analysis in Spike 2. PSD profiles of the field potential recordings filtered for the theta band (4 – 7 Hz) were generated by Fourier transform analysis (Hanning window, FFT size 2048, resolution 4.883 Hz) from each recording. The profiles were calculated from a 100 – 300 second section of the field potential trace displaying peak oscillatory activity, with the baseline power subtracted offline. Power spectrum analysis was performed to ascertain oscillatory power.